UNIVERSIDAD NACIONAL AUTÓNOMA DE MÉXICO

FACULTAD DE INGENIERÍA

Fractal Fractional Dual Porosity Diffusion Model

TESIS

Que para obtener el título de

Ingeniero Petrolero

P R E S E N T A

Noé Jesús Hernández Pérez

DIRECTOR DE TESIS

Dr. Rodolfo Gabriel Camacho Velázquez

Ciudad Universitaria, Cd. Mx., 2022

Abstract

Unconventional reservoirs are characterized by having a wide pore-size distribution, ranging from nanopores to hydraulic fractures. Given these heterogeneities, non-uniform flow behavior is likely to be developed, and new models considering these complexities should be sought. This research presents a fractal-fractional model to consider the anisotropy, heterogeneity, and anomalous diffusive flow, that may occur inside unconventional reservoirs. This is done by incorporating a more general flux law and power-law relationships.

Subdiffusive flow is considered in the fracture network inside the SRV. Time-fractional derivatives in the flux law model this anomalous diffusion behavior (fractional approach). Additionally, it is assumed that the stimulation induces certain fractal characteristics in between the propped hydraulic fractures. Inside this region, petrophysical properties and matrix block size are assigned through power-law relationships (fractal approach). The model is solved numerically through a finite difference scheme, the results show good agreement with existing numerical and analytical works.

The generated responses cannot be obtained with existing models when anisotropy-heterogeneity and anomalous diffusion are present. Thus, the typical slopes are not recovered when the fractal dimension (dmf), connectivity index (θ), and anomalous diffusion exponent (α) take other than normal diffusion values ($dmf = 1$, $\theta = 0$, $\alpha = 1$).

According to this study, the anomalous diffusion approach represents an alternative for analyzing well responses from complex systems. It is also shown that, when designing stimulation treatments, attention should be paid to increasing unpropped fracture density-connectivity.

To the best of the authors' knowledge, this is the first time that, the effect anisotropy and heterogeneity in unconventional reservoirs, is analyzed through a $3D$ combination of fractal-fractional diffusion.

Dedicatoria y Agradecimientos

Quiero agradecer al Dr. Rodolfo Camacho por guiarme y supervisarme. Me siento muy inspirado por su dedicación y entusiasmo. En todo momento conté con su apoyo para la elaboración de esta tesis. Gracias

Deseo expresar mi gratitud a los miembros del jurado. Sus sugerencias han sido de vital importancia para mejorar este trabajo.

Este escrito simboliza el término de mis estudios de licenciatura en la UNAM. Agradezco a esta institución, a mis profesores y amigos. Realmente disfruté mucho los momentos que compartimos.

Agradezco al programa conjunto de ExxonMobil y el Institute of International Education (iie), quienes a través del programa Beca ExxonMobil para la Investigación, me apoyaron para poder realizar esta tesis.

Así mismo agradezco al programa de becas de titulación de la UNAM.

Jacqueline, gracias por tu constante apoyo y amor. Te dedico este escrito.

Fimalmente, quiero agradecer a mi familia, cuyo soporte ha sido la pieza fundamental para concluir esta meta. No encuentro las palabras para agradecer lo que me otorgan. Les dedico este trabajo, mi querida familia.

Contents

Chapter 1

Introduction

Energy consumption is growing so quickly that conventional reserves alone cannot satisfy the demand. Currently, substantial hydrocarbon volumes are being produced from low permeability formations. Some of these rocks have pores so small or poorly connected that they almost inhibit fluid flow, shale, and tight rocks are common examples. Due to its abundance around the world, production from these formations may be taken global, as technology leaps out of North America (Webster, 2014).

1.1 Problem Statement

Fluid flow modeling is crucial to develop these resources. Several approaches have been applied and innovative improvements are still being developed. However, multiple challenges and unanswered questions remain unsolved.

Geologic considerations are of paramount importance. Highly contrasting porous media coexist inside the same rock.

Several experiments including: ultra-high-pressure mercury injection, back-scattered scanning electron microscopy, and atomic force microscopy have identified pores in the range of nanometers. These nano-paths give promote flow mechanisms that are typically negligible in conventional reservoirs. It is thought that those mechanisms are responsible for the mismatches when only advection (Darcy approach) is considered (Javadpour et al., 2009).

The exceeds from expected production rates in unconventional reservoirs can also be explained by the presence of natural fractures. Evidence encountered in outcrops, cores, logs and microseismic monitoring suggest that their presence in shale rocks should not be dismissed. (Gale et al., 2014).

Hydraulic fracturing has become a mandatory procedure to cost-effectively develop these reservoirs. Describing rock alterations that result from this procedure, should also become mandatory. Discrete approaches have proven not practical for most of the cases. Furthermore, tracking fracture propagation itself is not the information of interest, but its influences on rock's fluid-flow properties. In this sense, if some concepts on fractal theory are recovered, advantage can be taken from some special characteristics of the induced fracture network. Their randomness, irregularity, and self-similarity (Wang et al., 2017) suggest that they can be fractally described, and thus, power law relationships may govern the resulting alterations.

The variance in pore size distribution in these rocks severely limits the assumption of uniform flow. Instead, flow at multiple scales is developed. Different velocity fields, at each scale, coexist in these reservoirs. Consequently, pressure and rate responses will depart from normal diffusion trends.

Complex systems sometimes inhibit diffusion processes to follow Gaussian statistics, and thus, Fick's second law fails to describe the related transport behavior (Metzler and Klafter, 2000). By analogy Darcy's law may also be insufficient for complex reservoirs. Fluid flow can be sub-diffusive in case of flux impediment, or super-diffusive if the flux is facilitated (Holy, 2016). As an alternative to analyze flow in complex media, this anomalous diffusion behavior has been studied through fractional (non-integer order derivatives) flux laws (See Fomin, 2011; Raghavan, 2011; Chen and Raghavan, 2015; Ozcan, 2014; Albinali, 2016; Holy, 2016).

Despite some authors have suggested the fractional approach as an alternative for dual-porosity models (see Holy (2016), Holy and Ozkan (2017), Ozcan (2014)), we believe that the application of fractionality should be limited. It would be better to consider a dual-porosity idealization with the two media having different degrees of fractionality (see Albinali (2016) and Raghavan and Chen (2019)). In this sense we decided to include a source term representing other pore system not included as part of the fracture network. For simplicity, pseudosteady-state flow was considered for the transfer function. This formulation assumes that, as pressure in the fracture is disturbed, there is an instantaneous readjustment of matrix block pressure, therefore, there are no pressure gradients inside matrix blocks. In

this way, the flux is not a function of position on matrix blocks, it is only proportional to the pressure difference between matrix blocks, and fractures.

1.2 Research Objective

The objective of this research is to present an alternative fractal-fractional model to consider the anisotropy-heterogeneity and anomalous diffusive flow inside a dual-porosity Stimulated Reservoir Volume (SRV). The model considers 3D flow and is solved numerically through a finite difference scheme. Single phase flow of slightly compressible fluid of constant viscosity and compressibility is considered.

1.3 Thesis Organization

- Chapter 1 states the problem under consideration and establishes the objectives of this work.
- Chapter 2 provides a brief description of the works that were consulted.
- Chapter 3 provides the general concepts that support the use of fractal theory to describe reservoir non-uniform properties.
- Chapter 4 provides a brief introduction into diffusion works and describes how anomalous diffusion models arise. It also provides support on the use of anomalous diffusion ideas to describe flow in complex reservoirs.
- Chapter 5 briefly describes the mathematical model and its considerations.
- Chapter 6 presents the verification of the model. This is attained by reproducing Ozcan (2014) and Holy and Ozkan (2017) data.
- Chapter 7 analyzes the sensitivity of the model responses to all the involved parameters.
- Chapter 8 provides the concluding remarks that arise from the results and presents some recommendations for future works.
- Appendices A and B provide a detailed description of the model and its derivation.

Chapter 2

Literature Review

Gale et al. (2014) presented a study of natural fractures in shale plays. They concluded that attributes of natural fractures influence, in good or bad sense, depending on the morphology of the fractures, production from shale reservoirs. The study includes core and outcrop data.

Maxwell et al. (2002) presented microseismic monitoring examples of Barnet Shale formation. These examples show the complexities developed by the interaction between hydraulic fracture, and the pre-existing fracture networks. Evidence from microseismic studies (Daniels et al., 2007; Fisher et al., 2005; Xu et al., 2009) leads to the conclusion that the stimulation extends beyond the symmetric bi-wing planar crack geometry typically considered.

According to Wu (2017), a large proportion of the hydraulic fractures created during a stimulation treatment remain unpropped. These fractures either have a fracture width smaller than the size of the proppants, or are too far away from the wellbore where proppant cannot reach. Despite their low conductivity (2-4 orders of magnitude less than hydraulic fractures), they present a huge potential for production enhancement.

The aforementioned studies indicate that considering uniform properties beyond the propped hydraulic fracture might not be representative enough.

Given the characteristics of randomness, irregularity, and self-similarity, fracture branches are excellent candidates to be fractally described (Wang et al., 2017). Fractal geometry was employed by Wang et al. (2017) to characterize fracture networks based on microseismic data. They successfully matched microseismic events with fractal bifurcation patterns.

Conventional flow models of fractured reservoirs typically assume uniformly distributed, all interconnected fractures, and a mono-scale fracture set. These assumptions severely limit their application. Multiple improvements and modifications have been proposed, however, alternative models must be sought (Chang and Yortsos, 1990).

One promising approach to overcome the limitations of conventional fractured reservoirs idealizations can be found in fractal theory.

O'Shaughnessy and Procaccia (1985) addressed diffusion on fractal objects. Chang and Yortsos (1990) developed a model to describe the single-phase flow of slightly compressible fluid in a fractal reservoir. The formulation consists of a fractal object (fracture network) embedded in a Euclidian medium. Reservoirs with nonuniform fracture distribution, fractures at different scales, and varying degrees of interconnection can be modeled through this approach. Acuña and Yortsos (1995) simulated pressure transients in synthetic fractal networks of fractures. They found out that the wellbore pressure is a power-law function of time.

Flamenco-Lopez and Camacho-Velázquez (2003) derived an approximate analytical solution for dual-porosity systems, exhibiting fractal characteristics. Short- and long-time approximations were used to determine fractal parameters. They demonstrated that, by analyzing transient and pseudo-steady state responses, a Naturally Fractured Reservoir (NFR) exhibiting fractal characteristics can be fully described.

Cossio Santizo (2012) combined a fractal diffusivity equation with the trilinear Flow Model. They introduced a new semi-analytic solution for flow in a finite-conductivity vertical fracture. This model considers that porosity and permeability are functions of distance from the wellbore as in Chang and Yortsos (1990).

Fuentes-Cruz et al. (2014) introduced a flow model for fractured wells where nonuniform permeability is considered. Stimulation degree decreases with distance from the main fracture plane. According to their studies, due to the alteration, reservoir response departs significantly from the uniform permeability approach. They considered linear and exponential relationships to represent the varying permeability, and to avoid mathematical singularities that the fractal approach may lead to.

Not only fractal characteristics cause reservoir responses to depart from normal diffusion trends.

According to Camacho-Velázquez et al. (2008), diffusion process of fractal reservoirs is history dependent. Formulations such as the one presented by O'Shaughnessy and Procaccia (1985) cannot fully describe the anomalous diffusion properties of fractals. In fractally fractured systems, the history of flow plays an important role in all stages of production. Thus, temporal flux dependencies must be considered.

In addition, unconventional reservoirs consist of wide range of pore sizes, thus, transport mechanisms at different scales must be considered (Yucel Akkutlu and Fathi, 2012).

Several experiments confirm the existence of Nanopores in shale reservoirs (Javadpour et al., 2009). Given the smallness of these pore paths, other transport processes take relevance besides viscous flow, and thus, Darcy's law becomes insufficient (Javadpour et al., 2009). In general, production begins with usual gas flow, followed by gas desorption, and, finally, gas diffusion occurs in kerogen. This sequence suggests an advective-diffusive-desorptive equation (Javadpour et al., 2009).

Javadpour et al. (2009) suggested a theoretical approach to describe gas flow in nanopores (only diffusion and advection were considered). The introduction of the apparent permeability concept allowed him to formulate a Darcy-like equation so that it could ease be adapted into commercial reservoir simulators.

Yucel Akkutlu and Fathi (2012) investigated multiscale gas transport phenomena in organic-rich shale core samples. They showed that as pore-walls effects increase (which is an obvious condition of nanopores), the predicted gas transport is somewhat enhanced (compared to conventional parabolic velocity profile). Other transport phenomena such as the hopping of molecules by kerogen walls were also considered.

In view of the system's complexity and considering the above-mentioned studies, flow through these systems will depart from normal diffusion trends. The overall transport could be considered as an anomalous diffusion transport.

Metzler and Klafter (2000) presented a generalization of O'Shaughnessy and Procaccia (1985) equation by including a temporal-dependent flux. Although not emphasized, the model involves the incorporation of an additional parameter in that it requires a modification to either the conservation equation or to the flux law (Raghavan, 2011). This work and most of the consulted references modify the flux law.

Camacho-Velázquez et al. (2008) investigated the production-decline behavior of a NFR ex-

hibiting single and double porosity with fractal networks of fractures. Significant decline departures from the Euclidian model were identified when fractality is present. Also, these researchers presented for the first time in the petroleum literature the application of fractional temporal derivative, defined by Caputo, combined with the fractal description of the petrophysical properties to capture anomalous diffusion. Camacho-Velázquez et al. (2008) presented for the first time approximate analytical solutions, for both the fractal and fractional cases, at early and late times for transient and boundary-dominated flow periods, respectively. This research was based on Metzler and Klafter (2000), O'Shaughnessy and Procaccia (1985), and Chang and Yortsos (1990) works mainly.

Fomin (2011) presented two approaches for modeling diffusion in fractals. According to his formulations, this can be done by assuming a variable diffusivity coefficient which scales with a power law in the special coordinate and by introducing fractional differential equations. These two ideas form the base to derive the model developed in this work.

Raghavan (2011) described a constitutive equation which employs the concepts used to model continuous time random walk (CTRW). In this equation, the instantaneous flux is replaced by a time-convolved delayed flux which also considers waiting period times for random walkers. Raghavan and Chen (2013) addressed fractional diffusion in hydraulically fractured horizontal wells (finite conductivity fractures were considered). Chen and Raghavan (2015) analyzed the combined effects of fractional space and time terms in the flux law and examined the response at a fractured well. Situations that slow down diffusion (obstacles) are modeled by time-fractional diffusion equations. On the other hand, diffusion enhancement (highly conductive paths) is modeled by space-fractional diffusion equations. Raghavan and Chen (2016) addressed two-dimensional flow towards a horizontal well under sub-diffusion. Power law decline trends were identified at boundary-dominated flow periods.

Ozcan (2014) presented a trilinear anomalous diffusion (TAD) model. His purpose was to analyze the concept of anomalous diffusion, an alternative to the conventional dual-porosity formulations, for the SRV region (a time fractional formulation replaced the original dual porosity idealization). The model was validated with a Barnet field well example which was also employed by Brown et al (2011) to validate the trilinear dual porosity model. In this research, sub-diffusion degree (represented by α, the anomalous diffusion exponent) depends on flow interruptions in the fracture network by matrix elements. A sparsely fractured, tight-matrix and loosely connected fractures could cause a high degree of sub-diffusion ($\alpha \to 0$). However, when flow in the fracture network is not much hindered by the interruptions of the matrix, normal diffusion can be developed ($\alpha \to 1$).

Holy (2016) developed a numerical, anomalous-diffusion based flow model and investigated its applicability to fractured nanoporous formations, tight-oil or shale-gas plays. Holy (2016)'s approach claims that the extensive characterization (petrophysical properties and scale dependent transport mechanisms) required to accurately describe these reservoirs, can become impractical. Instead, a practical but rigorous alternative approach can be implemented by focusing on the response itself. Thus, fluid flow through these systems was modeled either as sub-diffusive (hindered flux) or supper-diffusive (facilitated flux). Three cases were considered: slightly compressible fluid (implicit scheme), compressible gas flow (implicit, simple iterative scheme), two-phase flow (Implicit Pressure Explicit Saturation scheme).This model considers one dimensional flow, and homogeneous phenomenological coefficient (permeability for normal diffusion) and porosity. A nonuniform mesh was latter considered in Holy and Ozkan (2017).

Albinali (2016) presented a solution for a trilinear flow scheme in a fractured horizontal well. Inside the SRV a dual-porosity idealization is considered. A fractional flux law is used to account for anomalous diffusion in fracture and matrix; different anomalous diffusion exponents for both media are considered. Normal diffusion is achieved by selecting appropriate values of anomalous diffusion parameters. The three contiguous linear flow regions coupled via pressure and flux continuity are considered.

Chu et al. (2017) carried out an extensive analysis of data from downhole pressure gauges in the Wolfcamp shale of the Permian basin. Using Chow pressure group, they identified power-law decline behaviors with slopes much different than conventional 1/2. Raghavan and Chen (2018) analyzed Chu et al. (2017) data through a modification of the transient-slab-matrix model of Kazemi (1969) or de Swaan O. (1976). Sub-diffusive flow is considered both in matrix and fracture network. Raghavan and Chen (2018) focuses on providing theoretical foundation to Chu et al. (2017) well responses. Chu et al. (2018) employed fractional diffusion solutions to interpret interference tests, power-law behaviors were also identified.

Raghavan and Chen (2019) went further by considering super and sub-diffusive flow in the fracture network, whereas only sub-diffusive flow was considered in the slab-matrix system. An analytical model was derived in Laplace domain.

Chapter 3

Overview of Fractal Theory

In a broad sense, fractals (natural and mathematical) are shapes that remain essentially unchanged as one zooms in continually (self-similarity is present at different scales).

3.1 Mathematical Fractals

Fractal geometry can also be considered as the study of geometric shapes that seem chaotic, but in fact perfectly orderly. This chaotic order arise from iteration of simple rules (Mandelbrot, 1989). See for example the Sierpiński triangle (3.1), which begins with an equilateral triangle (blue) which is recursively subdivided into smaller equilateral triangles (whiten).

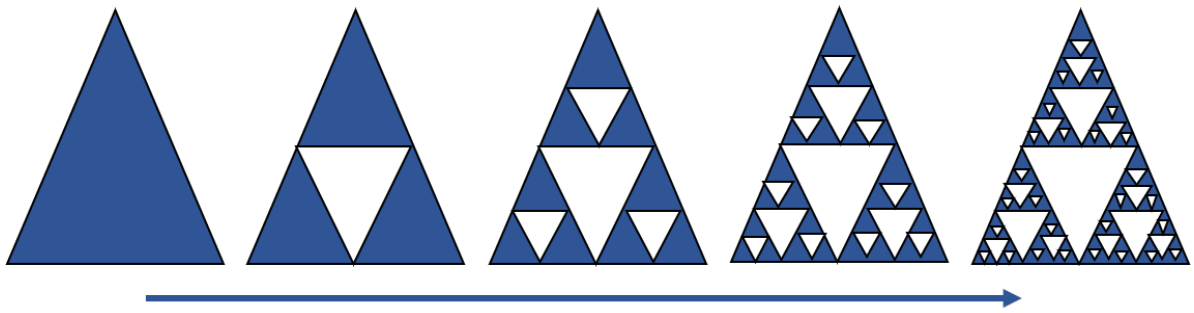

Figure 3.1: Sierpiński Carpet

For each generation step the area reduces by a factor of three quarters from the previous step. For the step n, the area will be $\left(\frac{3}{4}\right)^n$ of the zero step (original blue area). A different situation occurs to perimeter (interior side length). Each step, the perimeter is three halfs the previous step perimeter. For the n step, the triangle's perimeter will be $\left(\frac{3}{2}\right)^n$ of the zero step perimeter. As triangle goes further and further on its construction, the area will approach a zero value, but perimeter will keep growing. On the limit, as n goes to infinity, the figure will have a limited area but an infinite perimeter. Two methods are commonly employed to determine fractal dimension: the self-similarity method and the box counting method. With any of these methods it can be determined that the fractal dimension of the Sierpiński triangle is $dmf \simeq 1.585$, a number between one and two. The object shares features from one-dimensional and two-dimensional objects in some sense (depending on the step of the iteration process, from the two-dimensional triangle, $n = 0$, to the line segments, $n \to \infty$).

Strictly speaking, what is 'fractal' is not the figure itself, but rather a specific property of it (Cossio Santizo, 2012). For convenience, any object having fractal properties is also referred to as fractal.

3.2 Fractal Objects in Nature

Fractal, or fractal-like, objects also appear in nature. There are different natural phenomena which reflect certain scaling behavior and self-similarity. The scaling behavior is equivalent to saying that some property of the fractal can be described by a power-law relation (Hardy and Beier, 1994).

Fractals in nature can be considered as patterns repeated at different scales by natural processes. See for example the growth of a tree, each of its branches looks similar to the whole tree. Despite of the fact that each branch is much smaller (thin) than its predecessors, the pattern remains the same. Something similar happens with the structure of some leafs. Each vein grows in such a way that the bifurcation patterns are repeated at different scales. Three examples of fractals in nature are shown next

Figure 3.2: Fractals in Nature

Repetition patterns at different scales can also be found in the currents of a river delta, the growth of lightning, coast lines, snow flakes, and why not in hydraulic fractures? In some way, they all reproduce smaller and smaller copies of themselves as they grow. All these examples may look completely chaotic, however, because in a broad sense, the same process is repeated over and over again; the self-similarity within these fractal-like structures is much organized than it appears, in a statistical sense.

3.3 Hydraulic Fractures, Fractals in Nature?

When a hydraulic fracture treatment is carried out a huge amount of energy is delivered at the injection point. Rock begins to fail and fracture starts growing. The main propagation direction is dictated by in-situ stress, however, rock heterogeneity and the presence of natural fractures, provide weak paths where branches from the main fracture can arise. As the fluid moves away, less energy will be available and smaller branches will be created, yet, growth pattern will keep the same (smaller branches will continue growing through paths of weakness). The growth of trees and hydraulic fractures shares certain similarity. Both begin with a main trunk which spreads into smaller branches, whose size depends on the branching level/step/generation, i.e, its distance from the main trunk.

Once the fractures are created, the flow back process will leave the proppants behind. However, some branches will have a fracture width smaller than the size of the proppants or they will be too far away from the wellbore where proppant cannot reach (Wu, 2017). Proppant

density will decline with distance from the main fracture plane, with the highest density inside the main fracture plane. Here, proppant density refers to the number of grains inside the fracture, not to the material's density itself.

The main fracture plane will be propped and thus, uniform properties can be considered in this region. The decline in proppant density and stimulation degree suggest employing a nonuniform approach to assign properties inside the SRV. The enhancement in flow properties will decrease with respect to the distance from the main fracture plane. This behavior will continue up to the point where reservoir unstimulated properties are found (the point where energy was not enough to keep breaking down the rock).

Tracking the real growth of hydraulic fractures is quite complicated, Discrete Fracture Netowrk (DFN) models should be considered. A more practical approach is selected here.

Given that hydraulic fractures spread out following fractal patterns (see chapter 2 for more detail), a power-law model is considered to describe the non-uniformity of the SVR. Fractures in the SRV are not modeled themselves, in fact, just the concepts of fracture density and connectivity are considered. Reservoir permeability, porosity and matrix block size are correlated to fracture density and connectivity. Thus, these three parameters are assigned according to a power law relationship which depends on fracture density and connectivity in some way. The approach follows the ideas presented by Chang and Yortsos (1990), Acuña and Yortsos (1995), Camacho-Velázquez et al. (2008) and Cossio Santizo (2012).

In a broad sense, the power law relation is given as follows

$$P_s = \begin{cases} P_v \left[\left(\frac{x}{L_{S_x}} \right)^{b_x} \left(\frac{y}{L_{S_y}} \right)^{b_y} \left(\frac{z}{L_{S_z}} \right)^{b_z} \right] & \text{for } x \leq L_{S_x},\ y \leq L_{S_y},\ z \leq L_{S_z} \\ \\ P_v & \text{for } x > L_{S_x},\ y > L_{S_y},\ z > L_{S_z} \end{cases} \tag{3.1}$$

where P_s is the resultant value of a original property, P_v, after the stimulation treatment. The exponents b_x, b_y, b_z involve the fractal parameters (connectivity index θ, fractal dimension dmf and Euclidian dimension d). Note that the scaling behavior is only present inside the stimulated region delimited by $L_{S_x}, L_{S_y}, L_{S_z}$, outside of this region, original reservoir properties are found. Further detail is provided in chapter 5 and Appendix A.

Chapter 4

Overview of Fractional Diffusion

4.1 First Steps into Diffusion Models

By the first quarter of nineteenth century, Joseph Fourier had already studied the theory of heat propagation through solids. At the time, Laplace was trying to estimate the probability that the sum of n random variables may be equal to or less than a certain value when n is very large. Both the equations they formulated share similar forms (Narasimhan, 2009).

The study of diffusion also traces its roots back to Robert Brown and his observations of the erratic motion of particles. Unfortunately, because of the advancements at that time (1820s), Robert Brown was unable to provide further insight. (Turner, 2012).

A milestone in the field of diffusion came up from the work of Adolf Eugen Fick. This German physiologist presented a phenomenological approach to describe how particles under random motion tend to spread from a region of higher concentration to a region of lower concentration. He postulated the flux of matter ȷ in x direction is proportional to the pertaining gradient of concentration C. The constant of proportionality D was dependent upon substance nature (Narasimhan, 2009).

$$j = -D\frac{\partial C}{\partial x} \tag{4.1}$$

Currently, his theory and similar approaches are referred to as 'linear response' approaches (Narasimhan, 2009).

Combining equation 4.1 with conservation of matter, the Fick's second Law (Diffusion equa-

tion) is derived.

$$\frac{\partial C}{\partial t} = D\frac{\partial^2 C}{\partial x^2} \tag{4.2}$$

Fick's first Law 4.1 and the diffusion equation 4.2 were widely regarded as statements in continuum mechanics. The kinetic molecular hypothesis gained widespread acceptance only after Albert Einstein's famous analysis of Brownian motion in 1905 (Gillespie and Seitaridou, 2012).

4.2 Einstein Diffusion Equation

The following derivation is taken from Gillespie and Seitaridou (2012); for simplicity some steps have been omitted.

Lets consider a rectangular liquid (solvent) container where Brownian particles (solute) have been left (see figure 4.1). The number of solute particles at certain x-coordinate and certain time t is represented by $\rho(x,t)$. Now assume a time interval δt which is infinitesimal but also large enough to allow solute molecule to collide many times with solvent molecules. Those particle motions during different successive intervals are assumed independent from displacements in previous time steps. To describe the displacement that results from particle collisions, it means the likelihood of a particle to displace from a certain location to another, an stochastic approach is employed. Consider the probability density function of displacement $\phi(\zeta;\delta t)$, defined so that, it gives the probability that the x-coordinate of a solute molecule will change during the next δt by an amount between ζ and $\zeta + d\zeta$.

Now, to determine how many solute molecules will end up at a certain x-coordinate inside the enclosed area (limited by x and $x + dx$) for the next time interval $t + \delta t$, that is, $\rho\,(x, t+\delta t)\;\; dx$, the procedure presented by Gillespie and Seitaridou (2012) is applied.

$$\rho\,(x, t+\delta t)\;\; dx = \int_{\zeta=-\infty}^{\infty} \left[\rho\,(x-\zeta, t)\;\; dx\right] \times \left[\phi\,(\zeta, \delta t)\, d\zeta\right] \tag{4.3}$$

The factor $[\rho\,(x-\zeta,t)\;\; dx]$ represents the number of solute molecules in the dx-interval that are located at $x-\zeta$ at time t. Then, $[\phi\,(\zeta,\delta t)\, d\zeta]$ represents the fraction (in average) of solute molecules that will suffer a displacement (due to collisions with solvent molecules)

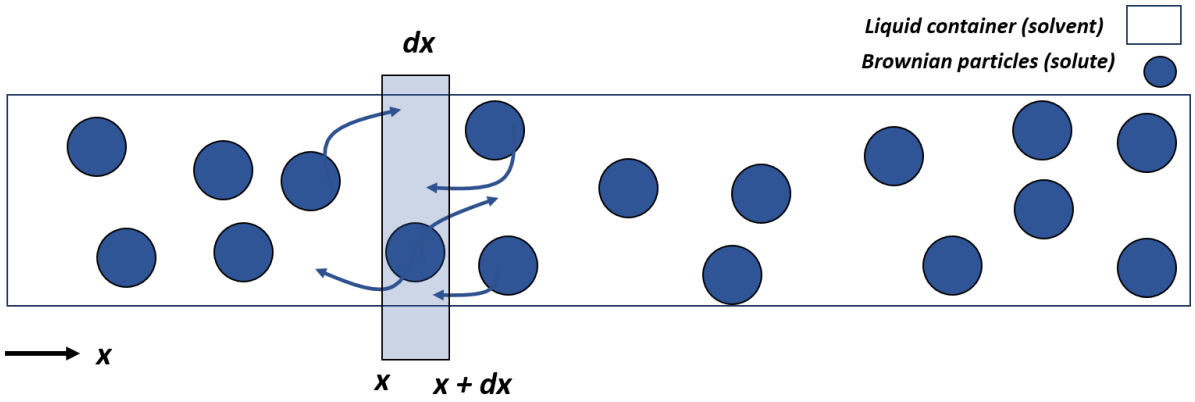

Figure 4.1: Brownian particles

in x-coordinate between ζ and $\zeta + d\zeta$ and will therefore end up in the dx-interval at x at time $t + \delta t$. The product is then summed (integrated) over all possible values of ζ to get the average number of molecules with x-coordinate between x and $x + dx$ at time $t + \delta t$.

From equation 4.3, dxs are canceled. Then, the term $\rho(x - \zeta)$ is Taylor expanded around x.

$$\begin{aligned} \rho(x, t + \delta t) &= \int_{\zeta=-\infty}^{\infty} \phi(\zeta, \delta t) \left[\rho(x, t) + \sum_{k=1}^{\infty} \frac{(-\zeta)^k}{k!} \frac{\partial^k \rho(x, t)}{\partial x^k} \right] d\zeta \\ &= \rho(x, t) \int_{\zeta=-\infty}^{\infty} \phi(\zeta, \delta t)\, d\zeta + \sum_{k=1}^{\infty} \frac{\partial^k \rho(x, t)}{\partial x^k} \left[\frac{1}{k!} \int_{-\infty}^{\infty} (-\zeta)^k \phi(\zeta, \delta t)\, d\zeta \right] \end{aligned} \tag{4.4}$$

As the total probability equals one, the integral in the first term of right hand equals one. Now, because the probability of displacement is symmetric, the negative and positive displacements are equally likely. This means that under the summation of many terms, all odd terms in the sum will add up to a zero net displacement. Then only even terms will be considered. According to Gillespie and Seitaridou (2012), the rearrangement of equation 4.4 results in

$$\frac{\rho(x, t + \delta t) - \rho(x, t)}{\delta t} = \sum_{k=1}^{\infty} \left[\frac{1}{\delta t} \frac{1}{(2k)!} \int_{-\infty}^{\infty} \zeta^{2k} \phi(\zeta, \delta t)\, d\zeta \right] \frac{\partial^{2k} \rho(x, t)}{\partial x^{2k}}. \tag{4.5}$$

Considering only the first term of the sum, the Einstein diffusion equation is obtained,

$$\frac{\partial \rho(x,t)}{\partial t} = D\frac{\partial^2 \rho(x,t)}{\partial x^2}, \tag{4.6}$$

where

$$D \equiv \frac{1}{2\delta t}\int_{-\infty}^{\infty} \zeta^2 \phi(\zeta, \delta t)\, d\zeta. \tag{4.7}$$

In 1908 Jean Perrin carried out a series of experiments which confirmed Einstein results and thus the molecular-kinetic theory.

The solution to the above diffusion equation turns out that the probability distribution is Gaussian in nature (normal). From Einstein's approach it can be concluded that the mean square displacement $\langle r^2(t)\rangle$ of a particle scales linearly with time.

$$\langle r^2(t)\rangle \propto t \tag{4.8}$$

4.3 Random Walk

Another way to deal with the erratic motion of particles is by considering that they behave as random walkers. Figure 4.2 shows a representation of the trajectory followed by two Brownian particles.

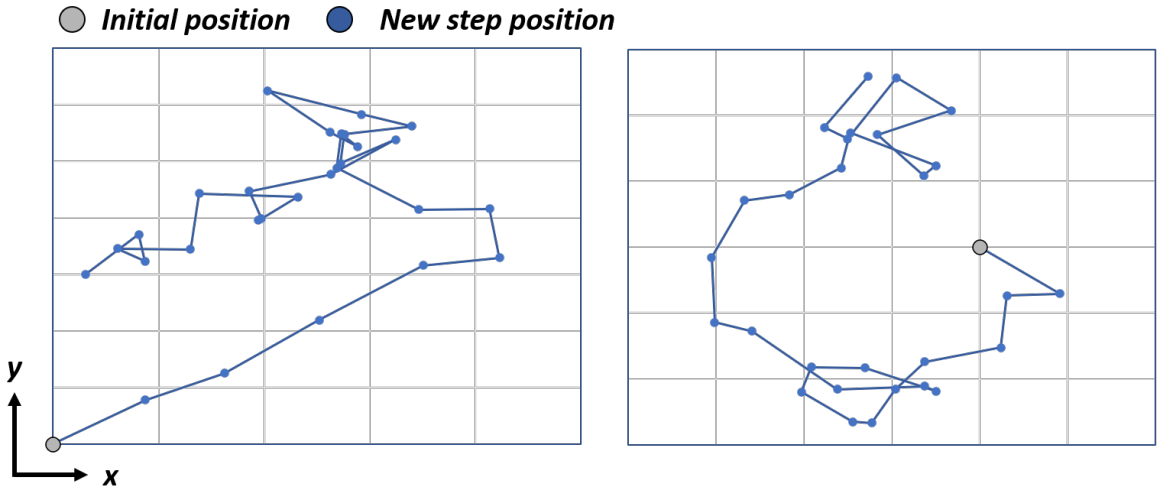

Figure 4.2: Simulation of Brownian particle Trajectory

According to Metzler and Klafter (2000), this erratic motion can be seen as a random walk. For the 2D-case, this model assumes that an individual can only move in four directions at each time step: right, left, up and down (see figure 4.3). Each displacement is independent from the previous ones. After a certain number of steps the individual will draw a complex trajectory, such as those presented previously (figure 4.2).

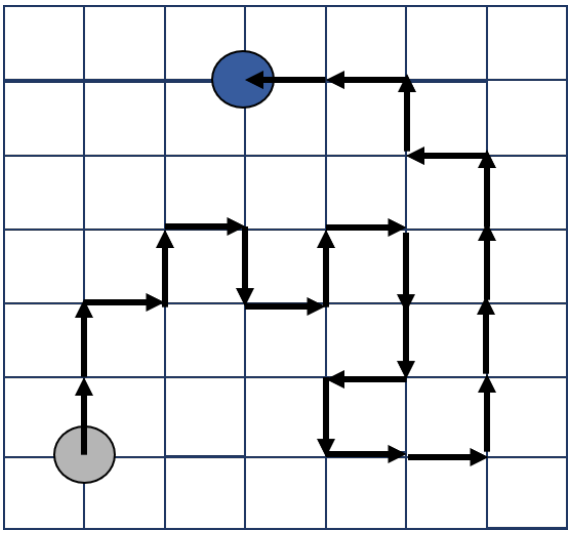

Figure 4.3: 2D Lattice for Random Walk, modified from Metzler and Klafter (2000)

For the following derivation, the one-dimensional case will be employed. Consider a random walker which can only move along a line. Its initial position is set at the origin and each time step (Δt) the walker has equal probability of displacing the same distance (Δx units), either to the right or to the left. Let's consider that $P(x,t)$ is the probability that the individual is at x at time t. Now the probability of finding the random walker at x at some time $t+\Delta t$ is given by

$$P(x,t+\Delta t) = \frac{1}{2}P(x-\Delta x,t) + \frac{1}{2}P(x+\Delta x,t)\,. \tag{4.9}$$

According to Metzler and Klafter (2000), the prefactor $1/2$, expresses the direction isotropy of the jumps. The probability of being at x in the next time step, $t+\Delta t$, is given by the sum of the probabilities of being at one jump (Δx), either to the right or to the left ($\pm\Delta x$), from the x-position just at time t.

Lets subtract $P(x,t)$ from both sides of the equation and divide by Δt

$$\frac{P(x,t+\Delta t) - P(x,t)}{\Delta t} = \frac{1}{2\Delta t}\left\{P(x-\Delta x,t) - 2P(x,t) + P(x+\Delta x,t)\right\}, \tag{4.10}$$

right hand side of the equation is multiplied by a unitary factor $(\Delta x^2/\Delta x^2)$,

$$\frac{P\left(x,t+\Delta t\right)-P\left(x,t\right)}{\Delta t}=\frac{\left(\Delta x\right)^2}{2\Delta t}\left\{\frac{P\left(x-\Delta x,t\right)-2P\left(x,t\right)+P\left(x+\Delta x,t\right)}{\left(\Delta x\right)^2}\right\}. \tag{4.11}$$

In the continuum limit $\Delta x, \Delta t \to 0$, considering that, under this limit, $\frac{(\Delta x)^2}{2\Delta t}$ is a constant, then, recalling finite-difference approximations, equation 4.11 can be written as follows

$$\frac{\partial P\left(x,t\right)}{\partial t}=D\frac{\partial^2 P\left(x,t\right)}{\partial x^2}, \tag{4.12}$$

where

$$D=\lim_{\Delta x\to 0,\Delta t\to 0}\frac{\left(\Delta x\right)^2}{2\Delta t}. \tag{4.13}$$

One more time, the diffusion equation is obtained. This random walk formulation also leads to a Gaussian shape, and to the conclusion that the Mean Square Displacement (MSD), scales with time in a linear way.

Although normal diffusion is one of the most fundamental process, many phenomena (see aquí poner papers de ejemplo) show deviations from normal diffusion trends. Slower (disorded solids, biological media, fractal media, porous media) or faster (turbulent plasmas, transport in polymers, Lévy flights) diffusion rates can be found in different environments (Henry et al., 2010). This anomalous diffusion behavior is characterized by scaling the MSD with a more general scaling form (Vlahos et al., 2008).

$$\left\langle r^2\left(t\right)\right\rangle \propto t^{\alpha} \tag{4.14}$$

The diffusion processes are then categorized according to the α-exponent in a power law relationship. Subdiffusion occurs when $0 \leq \alpha < 1$, superdiffusion cases are found when $1 < \alpha \geq 2$, and finally, if $\alpha = 1$ normal diffusion case is recovered.

This scaling behavior can also be linked to random walks, however, certain limitations of conventional random walks must be overcome.

4.4 Continuous Time Random Walks (CTRW), the Way to Anomalous Diffusion

The aim of this section is to present some conditions under which an experiment can lead to anomalous diffusion. This derivation is taken from Henry et al. (2010) and Metzler and Klafter (2000) mainly. Similar derivations can also be found in Sokolov and Klafter (2005), Vlahos et al. (2008) and Angstmann et al. (2013).

Classic random walks consider a constant length (Δx) jumps which successively occur at each constant interval time (Δt). To overcome these limitations, Montroll and Weiss in 1965 introduced the so called Continous Time Random Walks (CTRW). They considered that both, jump length and waiting time (the time elapsed between two successive jumps), are obtained from a probability density function (PDF), $\Psi\left(x-x',t-t'\right)$. This pdf represents the probability that a walker steps a jump length of $x-x'$ once it has waited a time $t-t'$.

Waiting times and jump lengths are independent identically distributed random variables, with density $\psi\left(t\right), t>0$ and $\lambda\left(x\right), x\in\mathbb{R}$ respectively. If the jump length and waiting time are independent from each other, then the decoupled form of the displacement PDF can be expressed as

$$\Psi\left(x-x',t-t'\right)=\psi\left(t-t'\right)\lambda\left(x-x'\right). \tag{4.15}$$

Now, according to Metzler and Klafter (2000) the survival probability, i.e., the probability that the walker does not jump during the time interval t, is given as

$$\Phi\left(t\right)=1-\int_0^t\psi\left(t'\right)dt'=\int_t^\infty\psi\left(t'\right)dt'. \tag{4.16}$$

The walker has not jumped since the expected waiting time is greater than t.

The fundamental quantity to calculate is PDF, $n\left(x,t\right)$, that a walker starting from whatever position be located at x at time t. This can related to following master equation of CTRW

$$n\left(x,t\right)=\Phi\left(t\right)n\left(x,0\right)+\int_{-\infty}^{\infty}\int_0^t n\left(x',t'\right)\psi\left(t-t'\right)\lambda\left(x-x'\right)dt'dx' \tag{4.17}$$

Equation 4.17 is the master equation for the expected concentration of walkers at x and time t. This equation relates the pdf $n(x,t)$ of just having arrived at position x at time t, with the event of having just arrived at x' at t', $n(x',t')$. The first term in the right hand side of the equation represents the persistence of the walker at the initial position. The second considers walkers that were at other positions x at time t' but then stepped to $\boldsymbol{x}$ at time t after waiting a time $t-t'$. All possible values of different jump lengths and waiting times are considered through the integration processes with respect to x' and t'.

4.5 The Quest for Anomalous Diffusion Equations

Different types of random walks arise depending on the way that jump lengths and waiting times are assigned, i.e., the way their PDF is defined. For the next, different options for jump length and waiting time densities will be considered.

4.5.1 Normal diffusion

According to Henry et al. (2010), the Fourier-Laplace (space-time) transform of the CTRW master equation is given as follows

$$\hat{\hat{n}}(q,s) = \hat{\Phi}(s)\,\hat{n}(q,0) + \hat{\psi}(s)\,\hat{\lambda}(q)\,\hat{\hat{n}}(q,s) \tag{4.18}$$

where s, and q denote the Laplace and Fourier variables respectively. Now, the Laplace transform of survival probability is given as

$$\hat{\Phi}(s) = \frac{1}{s} - \frac{\hat{\psi}(s)}{s} \tag{4.19}$$

Let's assume that jump lengths are Gaussian distributed

$$\lambda(x) = \frac{1}{\sqrt{2\pi\sigma^2}} \exp\left(-\frac{x^2}{2\sigma^2}\right) \tag{4.20}$$

Fourier transform of this pdf results in

$$\lambda(q) = \exp\left(-\frac{q^2\sigma^2}{2}\right) \tag{4.21}$$

Following Henry et al. (2010) procedure, the Taylor expansion of the previous equation results in

$$\lambda\hat{(}q) \sim 1 - \frac{q^2\sigma^2}{2} + O\left(q^4\right) \tag{4.22}$$

Now let's consider that waiting times are exponentially distributed with finite mean waiting time τ

$$\psi(t) = \frac{1}{\tau}\exp\left(-\frac{t}{\tau}\right) \tag{4.23}$$

The asymptotic expansion of the Laplace transform is given as

$$\hat{\psi}(s) \sim 1 - \tau s + O\left(s^2\right) \tag{4.24}$$

Equation 4.19, 4.22, 4.24 are substituted into equation 4.18 leads to

$$s\hat{\hat{n}}(q,s) = \left(1 - \hat{\psi}(s)\right)\hat{n}(q,0) + s(1-\tau s)\left(1 - \frac{q^2\sigma^2}{2}\right)\hat{\hat{n}}(q,s) \tag{4.25}$$

simplification of some terms results in

$$s\hat{\hat{n}}(q,s) = \tau s\hat{n}(q,0) + \left(s - \tau s^2\right)\left(1 - \frac{q^2\sigma^2}{2}\right)\hat{\hat{n}}(q,s) \tag{4.26}$$

and finally

$$s\hat{\hat{n}}(q,s) - \hat{n}(q,0) = -\left(\frac{\sigma^2}{2\tau}\right)q^2\hat{\hat{n}}(q,s) + s\left(\frac{q^2\sigma^2}{2}\right)\hat{\hat{n}} \tag{4.27}$$

The inverse Fourier and Laplace transforms the standard diffusion equation is recovered (Henry et al., 2010)

$$\frac{\partial n}{\partial t} = D\frac{\partial^2 n}{\partial x^2} \tag{4.28}$$

where

$$D = \frac{\sigma^2}{2\tau} \tag{4.29}$$

4.5.2 Subdiffusion

Following Henry et al. (2010) derivations, a Pareto waiting time density is considered,

$$\psi(t) = \frac{\alpha\tau^\alpha}{t^{1+\alpha}}\ t \in [\tau,\infty],\ 0 < \alpha < 1 \tag{4.30}$$

As this is a long-tailed distribution, the mean waiting time is infinite. In contrast to exponential case, this is a non-markovian distribution (waiting time density has temporal memory).

This should be also noted that this is a scale invariant distribution. (See Henry et al. (2010) for more detail)

The asymptotic expansion for this distribution is given by

$$\psi(s) \sim 1 - \Gamma(1-\alpha)\tau^{\alpha}s^{\alpha} \tag{4.31}$$

If a Gaussian pdf is considered for jump lengths, then the master equation for this CTRW can be written as follows

$$s\hat{\hat{n}}(q,s) - \hat{n}(q,0) = -\frac{\sigma^2}{2\tau^{\alpha}\Gamma(1-\alpha)}s^{1-\alpha}\hat{\hat{n}}(q,s) \tag{4.32}$$

taking the Fourier-Laplace inverse transform

$$\frac{\partial n(x,t)}{\partial t} = -D\mathcal{L}^{-1}\left(s^{1-\alpha}\frac{\partial^2 \hat{n}(x,s)}{\partial x^2}\right) \tag{4.33}$$

where

$$D = \frac{\sigma^2}{2\tau^{\alpha}\Gamma(1-\alpha)}. \tag{4.34}$$

Using rules of fractional integrals (these rules are under the scope of this chapter, but reader should refer to Henry et al. (2010) for more detail), the fractional order diffusion equation is obtained

$$\frac{\partial n(x,t)}{\partial t} = D\left({}_0\mathcal{D}_t^{1-\alpha}\frac{\partial^2 n(x,t)}{\partial x^2}\right) \tag{4.35}$$

${}_0\mathcal{D}_t^{1-\alpha}$ represents the Riemann-Liouville fractional derivative of order α. Finally, equation 4.35 represents the anomalous diffusion equation, for the subdiffusion case.

4.6 Waiting Time on Reservoirs?

Strictly speaking the overlap, or equivalency, of physical and stochastic diffusion models is limited to a narrow class of problems. Stochastic diffusion is designed to handle discrete objects moving randomly. However, some problems of physical diffusion are not associated with random motion, but with a driving force (pressure or concentration gradient). (Narasimhan, 2009).

Evidence suggests that some of the ideas developed for anomalous stochastic diffusion could be borrowed to model anomalous diffusion in porous media. This section explains the hypothesis which support the use of stochastic anomalous diffusion ideas to describe anomalous diffusion in complex reservoirs.

Let us start with the concept of waiting times. As it was previously shown, normal or anomalous diffusion can arise, depending on the waiting time pdf.

Some characteristics should be noted on normal distributions: they have some representative finite average of the system, so, they have a well defined center. Outside of this region, the distribution drop off exponentially fast; therefore, the probability of reaching extreme events is almost negligible. There are many phenomena well characterized by normal distributions; however, certain complex systems show a power law nature which is best suited with long-tailed distributions. Extraordinarily events are more likely to occur in Long-tailed distributions. As a result the representative average (mean) of the system diverges. As long-tailed distributions are power-law governed, they have the characteristic of being scale-free or scale invariant. Actually, the employment of these distributions to describe waiting time in CTRW has been referred to as fractal time random walk (Metzler and Klafter, 2000).

Long-tailed distributions are best suited to describe heterogeneous a systems.

Let us think about the system of studio that this work pretends to consider. Unconventional reservoirs (tight and shale) are characterized by having a wide pore size distribution, ranging from nanopores to hydraulic fractures (See chapter 2 for more detail). Flow in these reservoirs will be hindered by some paths of much lower conductivity. This can be seen as different waiting times for fluid to move. Some works have referred to waiting time as trapping time. Under this scope, trapping time is selected for better describing the link between CTRW ideas to reservoir engineering problems.

Of course, fluid trapping or flux impediments also occur in conventional reservoirs. However, the homogeneity in some of these reservoirs would allow them to be described by some representative (finite average) trapping time value, and thus, normal diffusion would govern flow in some of these reservoirs. In contrast, the heterogeneity of unconventional reservoirs inhibits to assign a mean trapping time to consider flux impediments. They are more likely to be described by a long-tailed distribution, and thus, the diffusion process would be sublinear (subdiffusion), i.e., the MSD would no longer scales with time linearly, and a more general (power-law) relation would be observed.

Although the anomalous diffusion equation presented above follows the trajectory of discrete walkers, an anomalous diffusion equation for a continuum environment could also be obtained through the application of an ad-hoc Darcy's Law (see Henry et al. (2010))

$$q = -\frac{k_\alpha}{\mu} \, {}_0\mathcal{D}_t^{1-\alpha} \, \frac{\partial p}{\partial x} \tag{4.36}$$

This phenomenological flux law is more general, computation of $\alpha = 1$ results in normal diffusion case. This should also be noted that k_α has units of $L^2T^{1-\alpha}$

4.7 Space Dependent Diffusion Coefficient

O'Shaughnessy and Procaccia (1985) presented a different approach to formulate an anomalous diffusion equation (for the case of fractal objects). A space dependent diffusion coefficient was employed instead of the constant one. This procedure changes the scaling relationship of MSD with time. One way of addressing this space deppendency is through the application of the fractal approach. However, as noted by Camacho-Velázquez et al. (2008), diffusion process of fractal reservoirs is history dependent, and thus, formulations such as the one presented by O'Shaughnessy and Procaccia (1985) cannot fully describe the anomalous diffusion properties of fractal reservoirs. In fractally fractured systems, the history of flow plays an important role in all stages of production. Thus, temporal flux dependencies must also be considered.

The two ideas presented in this chapter for addresing anomalous diffusion, fractionality and space dependent diffusion coefficient, form the base for the model developed.

Chapter 5

Model Description

Let us consider a horizontal well drilled in a rectangular reservoir originally consisting of two media: natural fractures (represented by subscript f) and matrix (represented by subscript m). Both media exhibit poor flow characteristics. Although natural-fracture-network permeability (k_f) is much larger than that of matrix (k_m), it is not large enough to allow production under profitable rates. Hydraulic fracturing is conducted, and higher conductivity paths are induced. For simplicity, a set of n_F (number of hydraulic fractures) equidistant and identical hydraulic fractures (represented by budscript F) is considered. See figure 5.1.

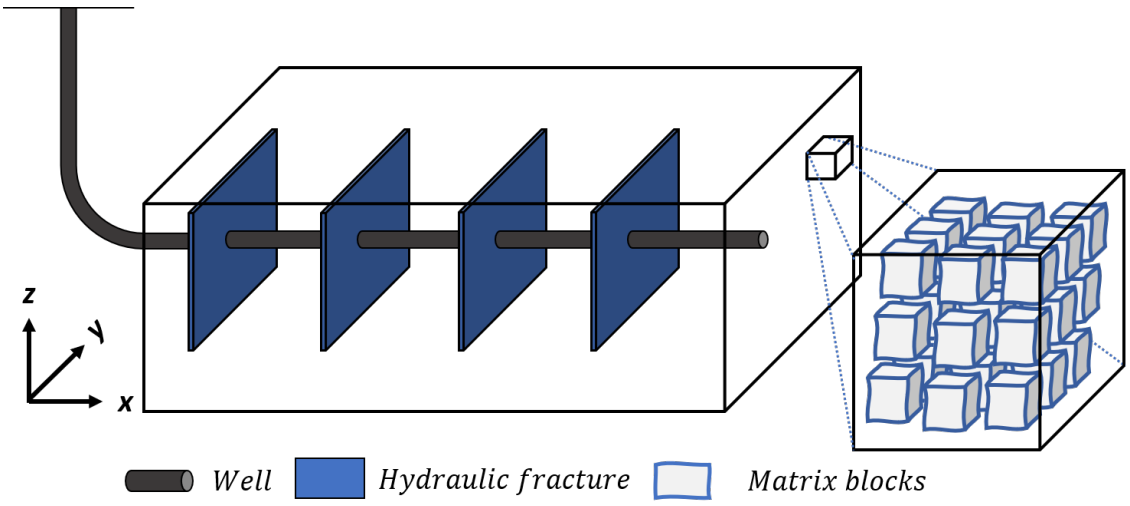

Figure 5.1: Typical fractured well in a 2ϕ reservoir

Typical representations of fractured wells consider that stimulation is only limited to the propped section of the hydraulic fracture (HF). For practical purposes this approach is valid, however, evidence suggests that a region of higher permeability is also created around HFs. Actually, the effectiveness of fracture treatment is often correlated with the SRV extent and associated permeability, as obtained from microseismic and flowback data (Agrawal et al., 2020). Some pre-existing natural fractures (NF) can be reactivated by the branches that propagate away from the main HFs.These fractures either have a fracture width smaller than the size of proppants, or are too far away from the wellbore, where proppant cannot reach (Wu, 2017). The absence of proppants causes them to have a much lower conductivity than the main HFs, but higher than that of the original fracture network (due to the stimulation).

A region of enhanced permeability surrounding the main HFs will be considered (see figure 5.2).

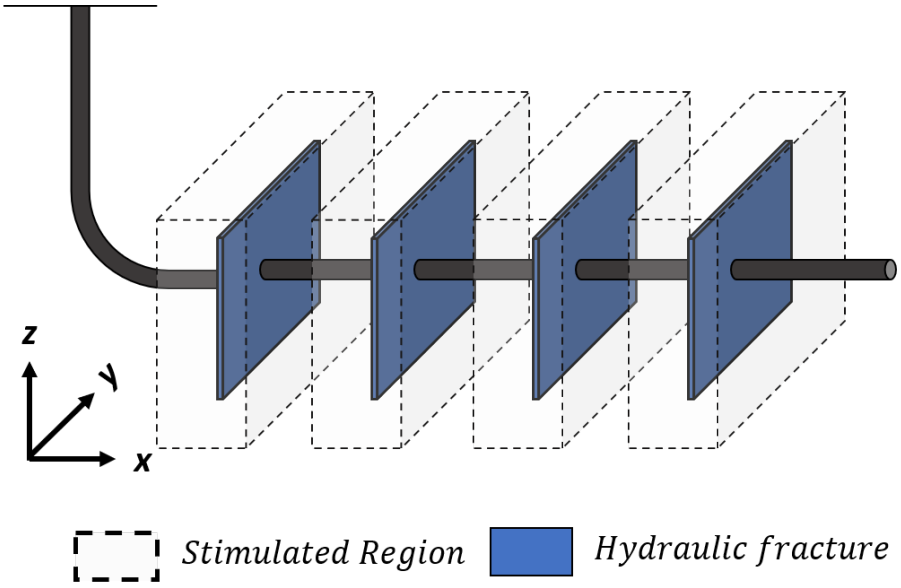

Figure 5.2: Schematization of a typical hydraulic stimulation

The symmetry of the problem enables us to consider only one eight of hydraulic fracture. The results from this section can be scaled up to each fracture and then to the well (see figure 5.3).

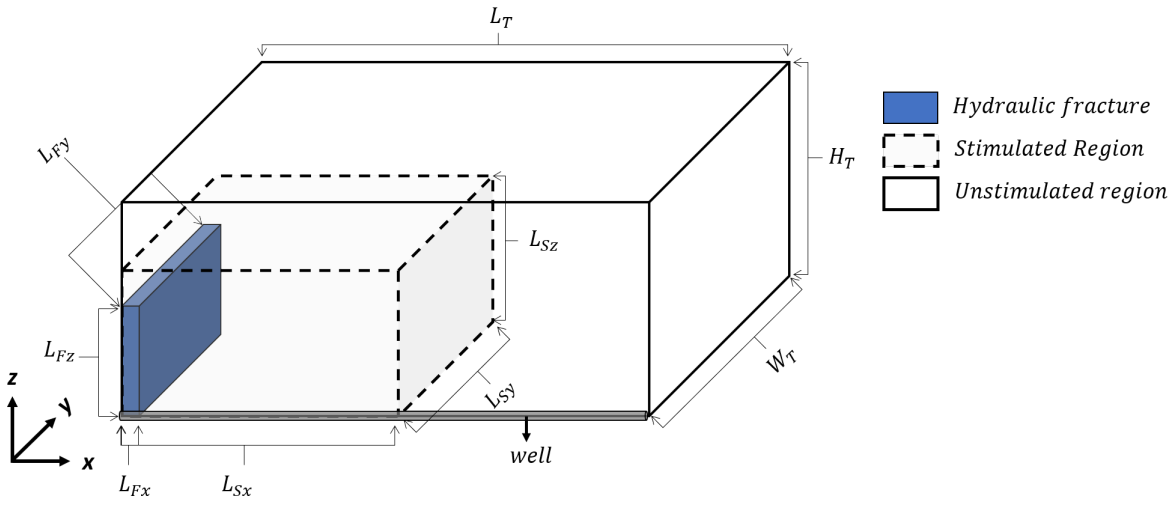

Figure 5.3: Problem domain reduction to one-eight section

5.1 Hydraulic Fracture

The model considers homogenous and isotropic properties inside the main plane of the HFs. As a result, normal diffusion is developed, and thus, the governing equation is given by

$$\frac{\partial}{\partial y}\left[\frac{k_F}{\mu}\frac{\partial p_F}{\partial y}\right] + \frac{\partial}{\partial z}\left[\frac{k_F}{\mu}\frac{\partial p_F}{\partial z}\right] = (\phi ct)_F \frac{\partial p_F}{\partial t} \tag{5.1}$$
$$for\ 0 > x < w_f/2,\ 0 > y < L_{Fy},\ 0 > z < L_{Fz}$$

The boundary conditions are depicted in figure 5.4

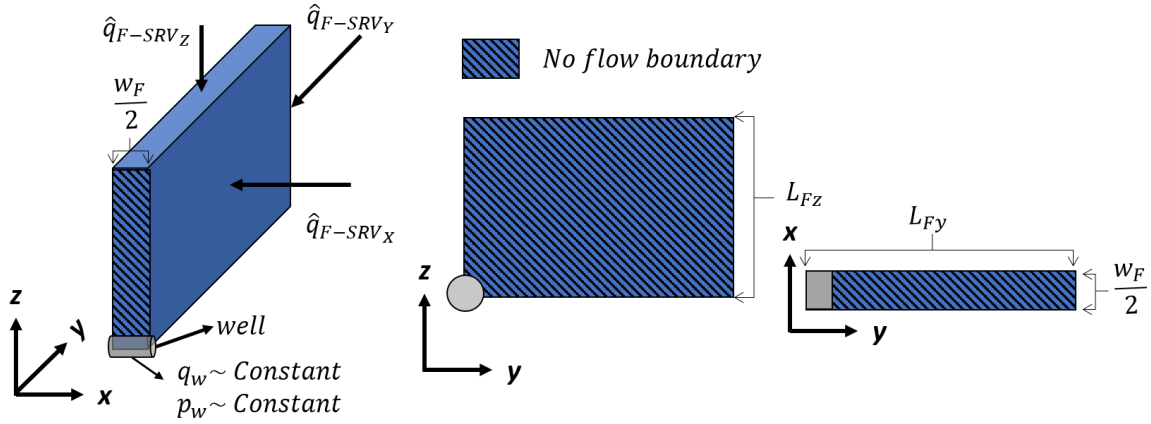

Figure 5.4: Hydraulic Fracture (HF) section

5.2 Stimulated Reservoir Volume and Outside Region

Stimulation magnitude decreases according to the distance from the main injection point. In this sense, non-uniform reservoir properties should be considered in the SRV (Figure 5.5).

The problem now is how to describe this non-uniformity. Fractal theory constitutes a promising approach on this regard.

Fractal structures are likely to arise in propagation of HFs. Bifurcation of main fracture branches will induce a certain fracture density which will increase as they propagate into the SRV. Despite fracture density would increase, the size of fractures and their impact on reservoir flow properties will decrease as the process goes on. This will continue up to the point where energy will be not enough to keep breaking the rock. A similar situation occurs in a fractal tree (see figure 3.2), where many branches result from a main trunk. As the process continues, the tree seems more populated but its branches are smaller and weaker. This decline in stimulation magnitude corresponds to a decline in SRV permeability and porosity. Matrix block size will also suffer changes but in a opposite way.

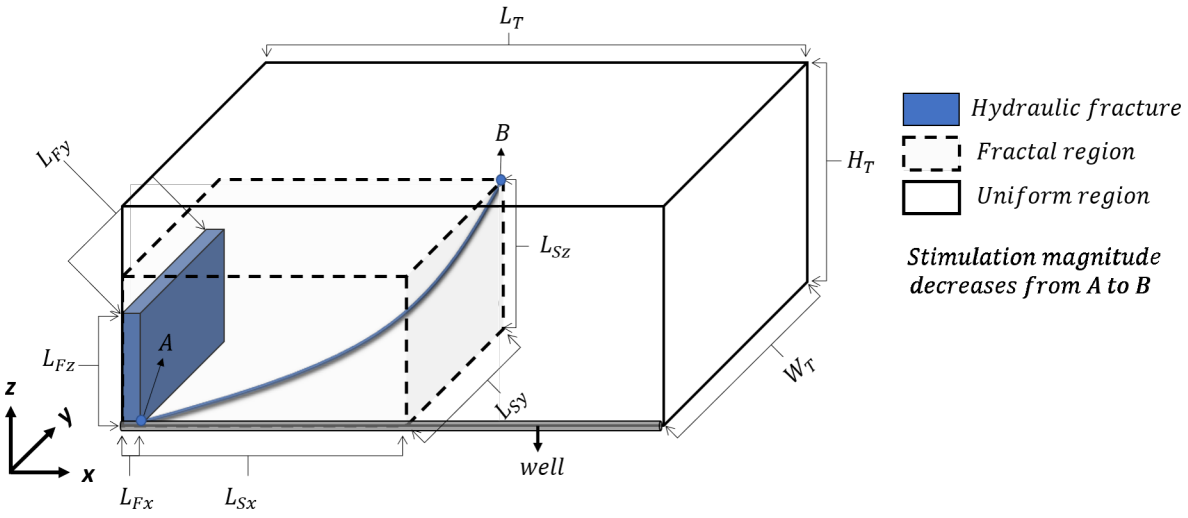

Figure 5.5: Stimulated Reservoir Volume (SRV)

The assignment of reservoir properties is performed with the following relations

- Phenomenological Flow Coefficient (permeability at α)

$$k_{\alpha,b_x} = \begin{cases} k_{\alpha,v_x}\left[\left(\frac{x}{L_{S_x}}\right)^{b_x}\left(\frac{y}{L_{S_y}}\right)^{b_y}\left(\frac{z}{L_{S_z}}\right)^{b_z}\right] & \text{for } x \le L_{S_x},\ y \le L_{S_y},\ z \le L_{S_z} \\ k_{\alpha,v_x} & \text{for } x > L_{S_x},\ y > L_{S_y},\ z > L_{S_z} \end{cases} \tag{5.2}$$

$$k_{\alpha,b_y} = \begin{cases} k_{\alpha,v_y}\left[\left(\frac{x}{L_{S_x}}\right)^{b_x}\left(\frac{y}{L_{S_y}}\right)^{b_y}\left(\frac{z}{L_{S_z}}\right)^{b_z}\right] & \text{for } x \le L_{S_x},\ y \le L_{S_y},\ z \le L_{S_z} \\ k_{\alpha,v_y} & \text{for } x > L_{S_x},\ y > L_{S_y},\ z > L_{S_z} \end{cases} \tag{5.3}$$

$$k_{\alpha,b_z} = \begin{cases} k_{\alpha,v_z}\left[\left(\frac{x}{L_{S_x}}\right)^{b_x}\left(\frac{y}{L_{S_y}}\right)^{b_y}\left(\frac{z}{L_{S_z}}\right)^{b_z}\right] & \text{for } x \le L_{S_x},\ y \le L_{S_y},\ z \le L_{S_z} \\ k_{\alpha,v_z} & \text{for } x > L_{S_x},\ y > L_{S_y},\ z > L_{S_z} \end{cases} \tag{5.4}$$

  where

$$b_x = dmf_x - \theta_x - 1 \tag{5.5}$$

$$b_y = dmf_y - \theta_y - 1 \tag{5.6}$$

$$b_z = dmf_z - \theta_z - 1 \tag{5.7}$$

- Porosity

$$\phi_c = \begin{cases} \phi_v\left[\left(\frac{x}{L_{S_x}}\right)^{c_x}\left(\frac{y}{L_{S_y}}\right)^{c_y}\left(\frac{z}{L_{S_z}}\right)^{c_z}\right] & \text{for } x \le L_{S_x},\ y \le L_{S_y},\ z \le L_{S_z} \\ \phi_v & \text{for } x > L_{S_x},\ y > L_{S_y},\ z > L_{S_z} \end{cases} \tag{5.8}$$

  where

$$c_x = dmf_x - 1 \tag{5.9}$$

$$c_y = dmf_y - 1 \tag{5.10}$$

$$c_z = dmf_z - 1 \tag{5.11}$$

- Matrix block size

$$L_x = \begin{cases} L_{v_x}\left[\left(\frac{L_{S_x}}{x}\right)^{c_x}\left(\frac{L_{S_y}}{y}\right)^{c_y}\left(\frac{L_{S_z}}{z}\right)^{c_z}\right] & \text{for } x \le L_{S_x},\ y \le L_{S_y},\ z \le L_{S_z} \\ \\ L_{v_x} & \text{for } x > L_{S_x},\ y > L_{S_y},\ z > L_{S_z} \end{cases} \tag{5.12}$$

$$L_y = \begin{cases} L_{v_y}\left[\left(\frac{L_{S_x}}{x}\right)^{c_x}\left(\frac{L_{S_y}}{y}\right)^{c_y}\left(\frac{L_{S_z}}{z}\right)^{c_z}\right] & \text{for } x \le L_{S_x},\ y \le L_{S_y},\ z \le L_{S_z} \\ \\ L_{v_y} & \text{for } x > L_{S_x},\ y > L_{S_y},\ z > L_{S_z} \end{cases} \tag{5.13}$$

$$L_z = \begin{cases} L_{v_z}\left[\left(\frac{L_{S_x}}{x}\right)^{c_x}\left(\frac{L_{S_y}}{y}\right)^{c_y}\left(\frac{L_{S_z}}{z}\right)^{c_z}\right] & \text{for } x \le L_{S_x},\ y \le L_{S_y},\ z \le L_{S_z} \\ \\ L_{v_z} & \text{for } x > L_{S_x},\ y > L_{S_y},\ z > L_{S_z} \end{cases} \tag{5.14}$$

Note that matrix block size should increase with distance from the main fracture plane.

As noted, the non-uniform properties are only assigned inside the stimulated region. Outside from this region, the properties remain essentially unchanged.

Both regions share the same governing equation, the only difference relies on the non-uniformity of reservoir properties. The governing equation is given as follows

$$\left\{ \begin{array}{c} \frac{\partial}{\partial x}\left[\frac{k_{(\alpha,b)_x}}{\mu}\frac{\partial^{1-\alpha}}{\partial t}\left(\frac{\partial p_f}{\partial x}\right)\right] + \frac{\partial}{\partial y}\left[\frac{k_{(\alpha,b)_y}}{\mu}\frac{\partial^{1-\alpha}}{\partial t}\left(\frac{\partial p_f}{\partial y}\right)\right] \\ \\ + \frac{\partial}{\partial z}\left[\frac{k_{(\alpha,b)_z}}{\mu}\frac{\partial^{1-\alpha}}{\partial t}\left(\frac{\partial p_f}{\partial z}\right)\right] - \ \hat{q}_{m-f} \end{array} \right\} = (\phi ct)_f \frac{\partial p_f}{\partial t} \tag{5.15}$$

The previous equation considers the anomalous diffusion behavior through the fractional flux law and space dependent (fractal) petrophysical properties. The source term indicates the matrix contribution. This is also a way of indicating that the application fractional approach, as a method of representing heterogeneity, should be limited. The transfer function is defined as follows

$$\hat{q}_{m-f} = \sigma_{SF}\ \frac{k_m}{\mu}\left(p_f - p_m\right) \tag{5.16}$$

All outside boundaries in the SRV and unstimulated regions are no flow boundaries, except for the boundaries between SRV and unstimulated regions.

Chapter 6

Verification of the Model

This section aims to verify the correctness of the Fractal-Fractional Dual-porosity Diffusion (FFDPD) model. Data obtained from existing numerical and analytical existing works were reproduced with the FFDPD model.

6.1 Ozcan (2014) Model

In this section, the FFDPD model will be verified against the Trilinear Anomalous Diffusion (TAD) solution, developed by Ozcan (2014).

The main idea of the TAD solution, is the replacement of the SRV dual-porosity idealization, by an anomalous diffusion approach. FFDPD and TAD models share certain similarities, their main difference relies on the dual-porosity considerations. The FFDPD model considers that, despite of the fact that by fitting an anomalous diffusion model, the extensive characterization would be avoided, a better description of the system is obtained by explicitly including most of its features.

A hypothesis of FFDPD model is that, the heterogeneity inside the fracture network, leads to anomalous diffusion (See chapter 4). Matrix blocks work as flux impediments, and they could induce different waiting times for fluids to move. One may think that this heterogeneity could be captured as part of the anomalous diffusion flow behavior, but the high contrast between matrix and fractures, severely limits this assumption. In this sense, the anomalous diffusion concept should be limited to avoid oversimplification; therefore, matrix contribution

should be considered explicitly. Albinali (2016) and Raghavan and Chen (2018) went further by considering different degrees of fractionality for matrix and fracture respectively.

Ozcan (2014) provided an example to show that the anomalous diffusion approach, can capture the behavior of a naturally fractured reservoir, idealized by a dual porosity model (See figure 3.1 of Ozcan (2014)). This example is useful to validate the FFDPD model because it allows to verify both, the implementation of the anomalous diffusion concepts, and the dual porosity formulation, separately. The anomalous diffusion side of the model is verified by turning down the dual-porosity formulation (FFDPD - Anomalous D), FFDPD collapses to TAD. Then, a normal diffusion case ($\alpha = 1, dmf = 0, \theta = 1$) is computed accounting only for the dual-porosity feature (FFDPD - 2 ϕ), the FFDPD collapses to the Trilinear Dual-Porosity model (TDP).

To verify the FFDPD model with this solution, fractal parameters must collapse to Euclidean case values.

Table 6.1 provides the general data computed, into the FFDPD, to reproduce the pressure responses shown in figure 3.2, and figure 5.1 of Ozcan (2014). Note that, k_m and k_f correspond to the normal-diffusion case permeability values. On the other side, k_α corresponds to the anomalous diffusion case, i.e., permeability at α. Ozcan (2014) considers one-dimensional flow in the x direction, for the SRV region, and one-dimensional flow in the y direction, for the HFs. Furthermore, only one quarter of the HF is modeled. Corresponding adjustments for wellbore rate, thickness and transmissibilities were carried out to reproduce these characteristics.

Figure 6.1 shows the results obtained when the FFDPD model is collapsed to the TAD solution of Ozcan (2014). Figure 3.1 from Ozcan (2014) was taken and modified to verify the FFDPD model. Figure 6.2 compares the results obtained with the FFDPD model and those of Ozcan (2014) when the anomalous diffusion exponent is modified. The models show good agreement.

Parameter	***Value***
Both figures	-
Constant wellbore flow rate, q_w, [stb/d]	15
Viscosity, μ, [cp]	0.3
Formation thickness, h, [ft]	250
Simulated thickness, H_T, [ft]	$h/2$
Distance to boundary parallel to well, W_T, [ft]	250
Hydraulic fracture half y-length, L_{Fy}, [ft]	W_T
Hydraulic fracture half z-length, L_{Fz},[ft]	H_T
Hydraulic fracture half width, L_{Fx}, [ft]	0.005
Hydraulic fracture porosity, ϕ_F,[1]	0.38
Hydraulic fracture permeability, k_F, [md]	5e4
Hydraulic fracture total compressibility, ct_F,[1/psi]	1e-4
Figure 6.1	-
Half distance between hydraulic fractures, L_T,[ft]	100
SRV reservoir x-permeability at α, k_{α,v_x}, [md-hr$^{1-\alpha}$]	1,200
SRV porosity-compressibility product, $(\phi\ c_t)_f$, [1/psi]	4.62 e-4
.....	.....
Matrix permeability, k_m, [md]	1e-4
Matrix porosity, ϕ_m, [1]	0.05
Matrix total compressibility, ct_m, [1/psi]	1e-5
Undisturbed matrix block size, L_{vx}, L_{vy}, L_{vz}, [ft]	1,1,1
Figure 6.2	-
Half distance between hydraulic fractures, L_T,[ft]	300
SRV reservoir x-permeability at α, k_{α,v_x}, [md-hr$^{1-\alpha}$]	1.2
SRV porosity-compressibility product, $(\phi\ c_t)_f$, [1/psi]	4.62 e-4

Table 6.1: Model verification - figure 6.1

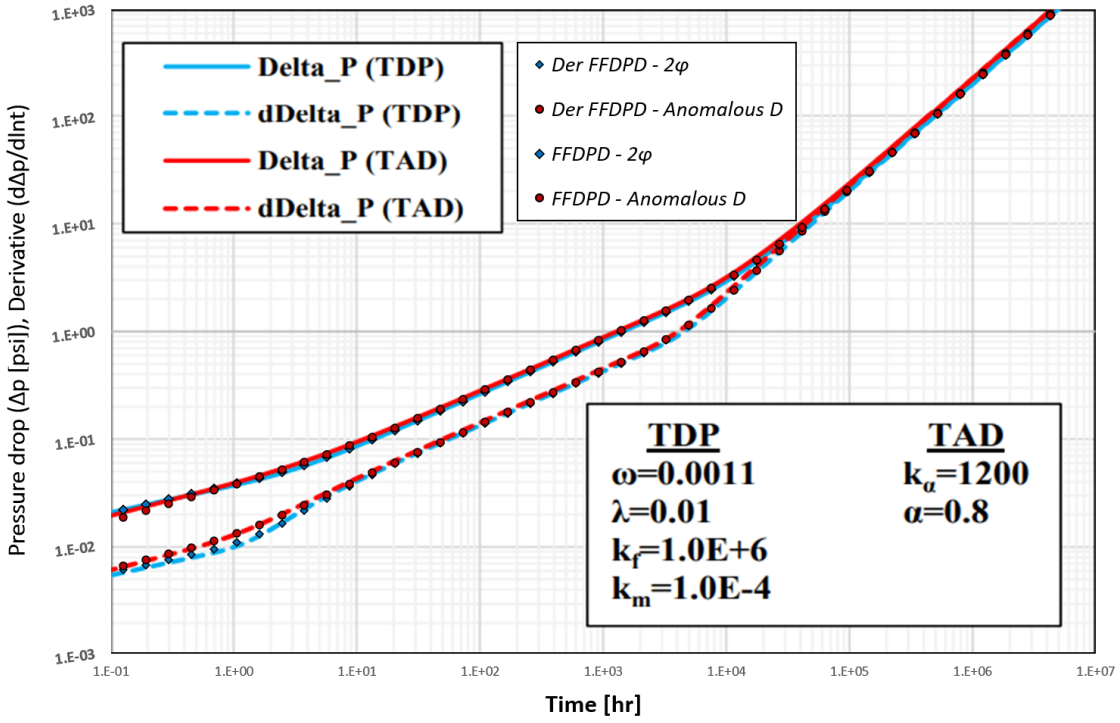

Figure 6.1: Model verification, modified from Ozcan (2014)

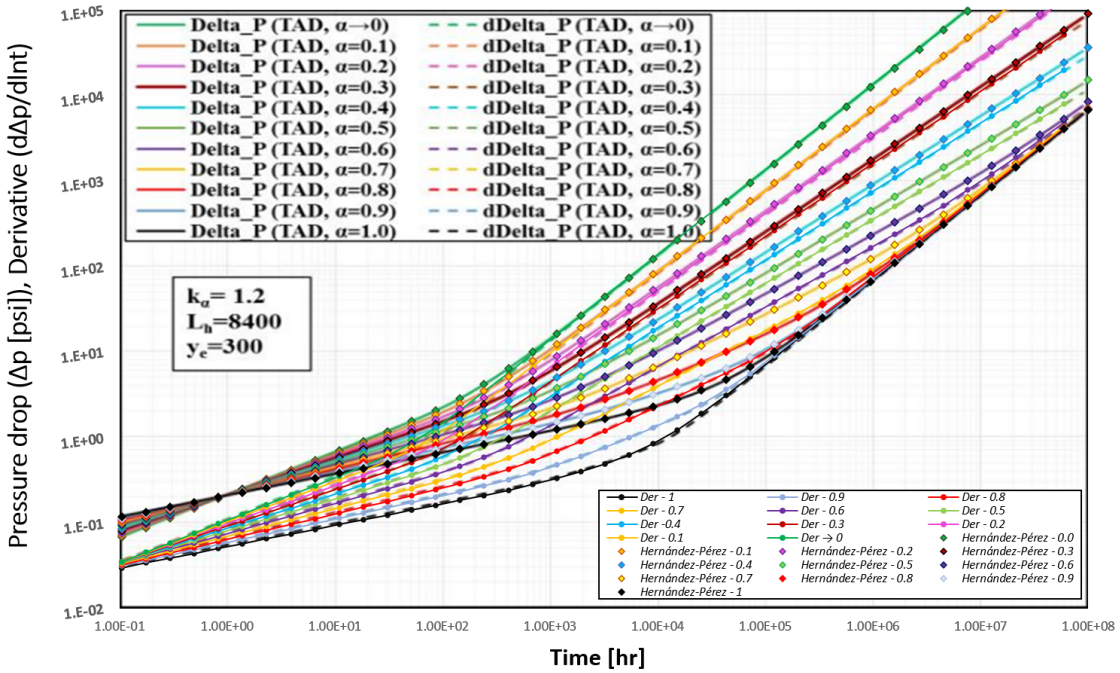

Figure 6.2: Model verification, modified from Ozcan (2014)

6.2 Holy and Ozkan (2017) Model

In this section the FFDPD model will be verified against the numerical model developed by Holy and Ozkan (2017). Holy (2016) considered that the responses from unconventional reservoirs could be analyzed with an anomalous diffusion approach, without rigorously assigning properties of matrix and fracture network. The model was latter enhanced by considering a non-uniform mesh in Holy and Ozkan (2017). To reproduce the responses of figure 2 (left) from Holy and Ozkan (2017), a one-dimensional flow grid is constructed and parameters are adjusted so that uniform properties be considered. Finally, as in Holy and Ozkan (2017) the responses are calculated at fracture face, hydraulic fracture cells are avoided.

Table 6.2 provides the general data computed into the FFDPD model to reproduce figure 2 (left) from Holy and Ozkan (2017).

Figure 6.3 demonstrates that both models exhibit excellent agreement.

Parameter	***Value***
Constant HF rate, q_w, [stb/d]	15
Viscosity, μ, [cp]	0.3
Formation thickness, h, [ft]	150
Simulated thickness, H_T, [ft]	$h/2$
Half distance between hydraulic fractures, L_T,[ft]	150
Distance to boundary parallel to well, W_T, [ft]	250
Hydraulic fracture half y-length, L_{Fy}, [ft]	W_T
Hydraulic fracture half z-length, L_{Fz},[ft]	H_T
SRV reservoir x-permeability at α, k_{α,v_x}, [md-d$^{1-\alpha}$]	0.05
SRV porosity, ϕ_f, [1]	0.2
SRV total compressibility, c_{tf}, [1/psi]	4e-5

Table 6.2: Model verification - figure 6.3

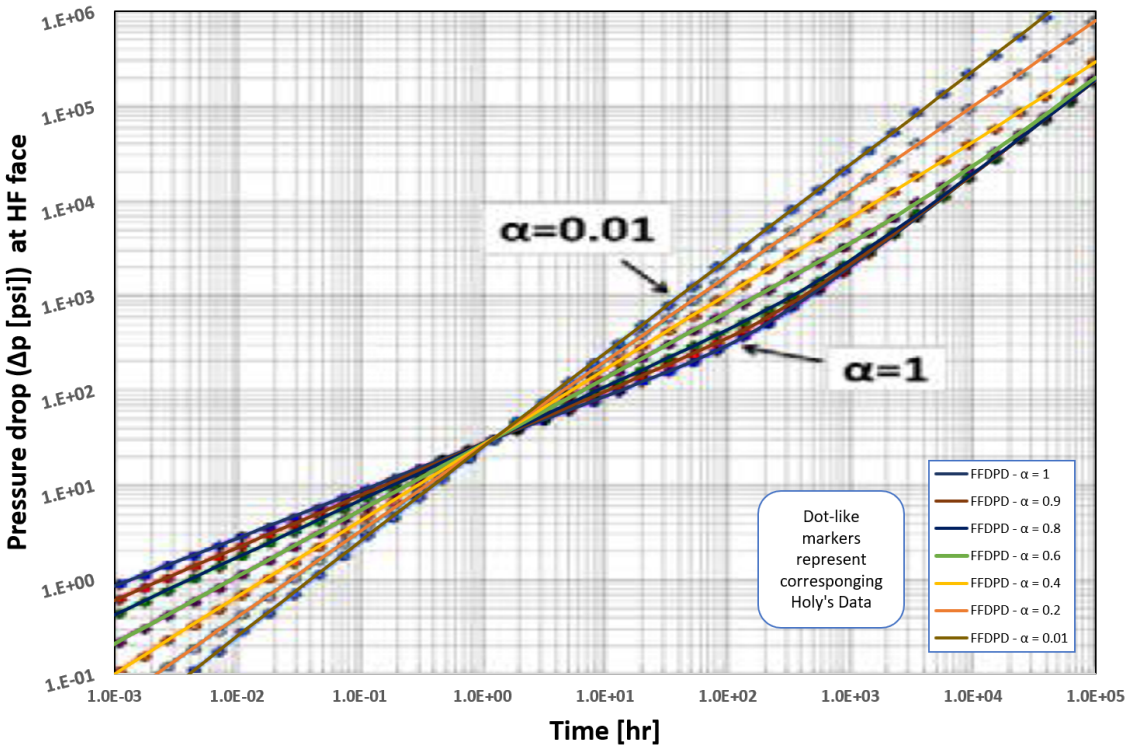

Figure 6.3: Model verification, modified from Holy and Ozkan (2017)

The Fractal-Fractional Dual-porosity Diffusion (FFDPD) model was verified and good agreement was obtained with existing numerical and analytical models.

Chapter 7

Results

In this chapter the results of the study are presented and analized with reference to the main objectives. In this sense, the sensitivity of the FFDPD model to the main parameters is evaluated.

Table 7.1 includes the general input data required to reproduce the pressure responses (figures 7.1, 7.2 and 7.3). Table 7.2 provides the general data for figure 7.4

Figure 7.1 shows the case of reservoir where a low fracture density ($dmf = 0.7$) and poor connectivity ($\theta = 0.1$) has been induced. The anomalous diffusion exponent aims to capture the degree of heterogeneity, between the several paths available for the fluids to flow, inside the fracture network. Those cases where the different flow paths (preexisting and induced during stimulation) are highly contrasting, inhibit the development of a uniform flow, and thus anomalous diffusion is developed. On the other hand, for homogeneous reservoirs normal diffusion will occur ($\alpha \rightarrow 1$). Of course, the more subdiffusive the process is, the more pressure drop (driving force) it will require, to maintain the imposed constant-rate condition.

Figure 7.2 shows the example of a reservoir with different degrees of fracturing developed during the stimulation (variable dmf). All the examples show a poor degree of connectivity ($\theta = 0.1$). Fractal dimension (dmf) was selected the same for all directions. The examples are still anisotropic because of the permeability vector at unstimulated conditions. Anomalous diffusion exponent was selected to represent a certain degree of subdiffusion.

Figure 7.3 reports the case of a poorly stimulated reservoir (Low fracture density has been induced, $dmf = 0.8$). The few flow paths show different degrees of connectivity (variable θ).

Connectivity index was selected the same for all directions; the examples are still anisotropic due to the unstimulated permeability vector ($k_{\alpha,v}$). Anomalous diffusion exponent was selected to represent a certain degree of anomalous diffusion.

Rate decline responses are discussed next.

Table 7.2 provides the general data required for reproducing figure 7.4. This example reports the case of a poorly stimulated reservoir. Fracture density as well as connectivity are both extremely low ($dmf \rightarrow 1$ and $\theta \rightarrow 0$).The anomalous diffusion exponent (α) reflects different degrees of heterogenities. As flow conditions deflect from normal diffusion, wells will decline faster, with differences in orders of magnitud.

Table 7.3 provides the general data employed in developing figure 7.5 and 7.6.

Figure 7.5 shows examples having different degrees of fracturing all having poor connectivity. Anomalous diffusion exponent was selected to represent some degree of heterogeneity inside all the examples. Very optimistic intial production rates are obtained when the medium is densily fractured, however, these cases show a faster decline. Initial production rates lower as fracturing level diminishes. Note that the differences are in order of magnitudes, both in time and rate. According to this figure, increasing fracture density far away from the propped sections, it is of paramount importance when designing stimulation treatments.

Figure 7.6 reports the case of a slightly fractured reservoir showing different connectivity levels. All examples exhibit almost neglible contrast in the magnitude of the rock flow properties ($\alpha = 0.9$). The cases where connectivity is high show a high initial production which declines faster, as compared with poorly connectivity cases. It is concluded form this figure that, when designing a fracture treatment, attention should be pay on increasing the connectivity behind the propped sections. Not only on the induced fractures, but for those already present.

As it can be seen in the figures, the usual slope patterns are not recovered when anomalous diffusion is present.

Note that there is a paradigm shift with respect to the tendencies in carbonate naturally fractured fractal reservoirs (NFFR). It is more feasible to have certainty on the value of reservoir original properties, than on the ones obtained at the HF face after stimulation treatment. Thus, in order to create the fractal distributions, the unstimulated reservoir properties are computed as the scaling parameters in the power law equations. It implies

that, for this study, the euclidian case ($dmf = 1, \theta = 0$) is in fact the unstimulated one. In other words, the euclidian case considers no stimulation is obtained beyond the HF, and thus, the most pesimistic case is obtained when euclidian parameters are computed. In contrast, for carbonate NFFR, the ideal or most optimistic case (Warren and Root model), is recovered through computation of euclidian values of fractal parameters ($dmf = 1, \theta = 0$).

Note also that simulation time is long, and some trends are highly optimistic. This is done mostly to provide a better visualization of the trends, and to provide a frame of reference with previous existing works, as we tried to employ similar data.

Parameter	***Value***
Constant wellbore flow rate, q_w, [stb/d]	150
Number of Hydraulic fractures, n_F,[1]	10
Viscosity, μ, [cp]	0.3
Formation thickness, h, [ft]	250
Simulated thickness, H_T, [ft]	$h/2$
Half distance between hydraulic fractures, L_T,[ft]	300
Distance to boundary parallel to well, W_T, [ft]	250
Hydraulic fracture half width, L_{Fx}, [ft]	0.005
Stimulated length on x-direction, L_{Sx}, [ft]	50
Hydraulic fracture half y-length, L_{Fy},[ft]	150
Stimulated length on y-direction, L_{Sy}, [ft]	200
Hydraulic fracture half z-length, L_{Fz}, [ft]	50
Stimulated length on z-direction, L_{Sz}, [ft]	20
Hydraulic fracture porosity, ϕ_F,[1]	0.38
Hydraulic fracture permeability (isotropic), k_F, [md]	5e4
Hydraulic fracture total compressibility, ct_F,[1/psi]	1e-4
Original reservoir x-permeability at α, k_{α,v_x}, [md-hr$^{1-\alpha}$]	3
Original reservoir y-permeability at α, k_{α,v_y}, [md-hr$^{1-\alpha}$]	$\frac{1}{5}k_{\alpha,v_x}$
Original reservoir z-permeability at α, k_{α,v_z}, [md-hr$^{1-\alpha}$]	$\frac{1}{10}k_{\alpha,v_x}$
SRV porosity-compressibility product, $(\phi\ c_t)_f$, [1/psi]	4.62 e-4
Matrix permeability, k_m, [md]	1e-4
Matrix porosity, ϕ_m, [1]	0.05
Matrix total compressibility, c_{tm}, [1/psi]	1e-5
Undisturbed matrix block size, L_{vx}, L_{vy}, L_{vz}, [ft]	1,1,1

Table 7.1: General data for figures 7.1, 7.2 and 7.3

Parameter	***Value***
Constant wellbore pressue drawdown, p_w, [psi]	900
Number of Hydraulic Fractures, n_F, [1]	5
Viscosity, μ, [cp]	0.3
Formation thickness, h, [ft]	300
Simulated thickness, H_T, [ft]	$h/2$
Half distance between hydraulic fractures, L_T,[ft]	250
Distance to boundary parallel to well, W_T, [ft]	250
Hydraulic fracture half width, L_{Fx}, [ft]	0.005
Stimulated length on x-direction, L_{Sx}, [ft]	80
Hydraulic fracture half y-length, L_{Fy},[ft]	40
Stimulated length on y-direction, L_{Sy}, [ft]	80
Hydraulic fracture half z-length, L_{Fz}, [ft]	40
Stimulated length on z-direction, L_{Sz}, [ft]	80
Hydraulic fracture porosity, ϕ_F,[1]	0.2
Hydraulic fracture permeability (isotropic), k_F, [md]	1e4
Hydraulic fracture total compressibility, ct_F,[1/psi]	1e-4
Original reservoir x-permeability at α, k_{α,v_x}, [md-hr$^{1-\alpha}$]	0.5
Original reservoir y-permeability at α, k_{α,v_y}, [md-hr$^{1-\alpha}$]	$\frac{1}{2}k_{\alpha,v_x}$
Original reservoir z-permeability at α, k_{α,v_z}, [md-hr$^{1-\alpha}$]	$\frac{1}{5}k_{\alpha,v_x}$
SRV porosity-compressibility product, $(\phi\ c_t)_f$, [1/psi]	4.62 e-4
Matrix permeability, k_m, [md]	1e-4
Matrix porosity, ϕ_m, [1]	0.05
Matrix total compressibility, c_{tm}, [1/psi]	1e-5
Undisturbed matrix block size, L_{vx}, L_{vy}, L_{vz}, [ft]	1,1,1

Table 7.2: General data for figure 7.4

Parameter	***Value***
Constant wellbore pressue drawdown, p_w, [psi]	900
Number of Hydraulic Fractures, n_F, [1]	5
Viscosity, μ, [cp]	0.3
Formation thickness, h, [ft]	100
Simulated thickness, H_T, [ft]	$h/2$
Half distance between hydraulic fractures, L_T,[ft]	100
Distance to boundary parallel to well, W_T, [ft]	100
Hydraulic fracture half width, L_{Fx}, [ft]	0.005
Stimulated length on x-direction, L_{Sx}, [ft]	20
Hydraulic fracture half y-length, L_{Fy},[ft]	10
Stimulated length on y-direction, L_{Sy}, [ft]	30
Hydraulic fracture half z-length, L_{Fz}, [ft]	10
Stimulated length on x-direction, L_{Sz}, [ft]	30
Hydraulic fracture porosity, ϕ_F,[1]	0.2
Hydraulic fracture permeability (isotropic), k_F, [md]	1e3
Hydraulic fracture total compressibility, ct_F,[1/psi]	1e-4
Original reservoir x-permeability at α, k_{α,v_x}, [md-hr$^{1-\alpha}$]	0.5
Original reservoir y-permeability at α, k_{α,v_y}, [md-hr$^{1-\alpha}$]	$\frac{1}{2}k_{\alpha,v_x}$
Original reservoir z-permeability at α, k_{α,v_z}, [md-hr$^{1-\alpha}$]	$\frac{1}{5}k_{\alpha,v_x}$
SRV porosity-compressibility product, $(\phi\ c_t)_f$, [1/psi]	4.62 e-4
Matrix permeability, k_m, [md]	1e-4
Matrix porosity, ϕ_m, [1]	0.05
Matrix total compressibility, c_{tm}, [1/psi]	1e-5
Undisturbed matrix block size, L_{vx}, L_{vy}, L_{vz}, [ft]	1,1,1

Table 7.3: General data for figures 7.5 and 7.6

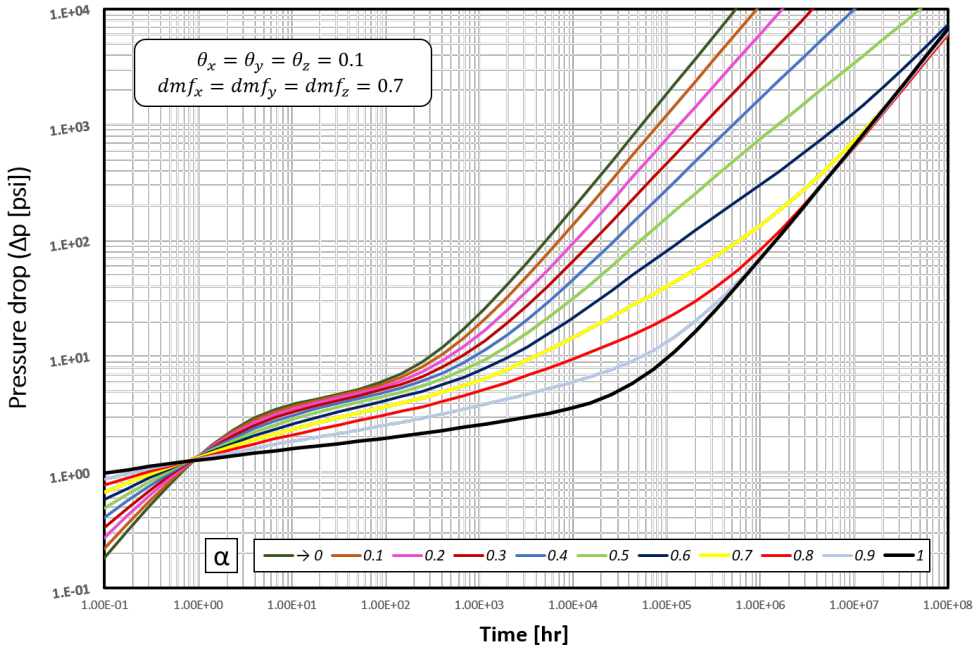

Figure 7.1: Pressure sensitivity: anomalous diffusion exponent, α

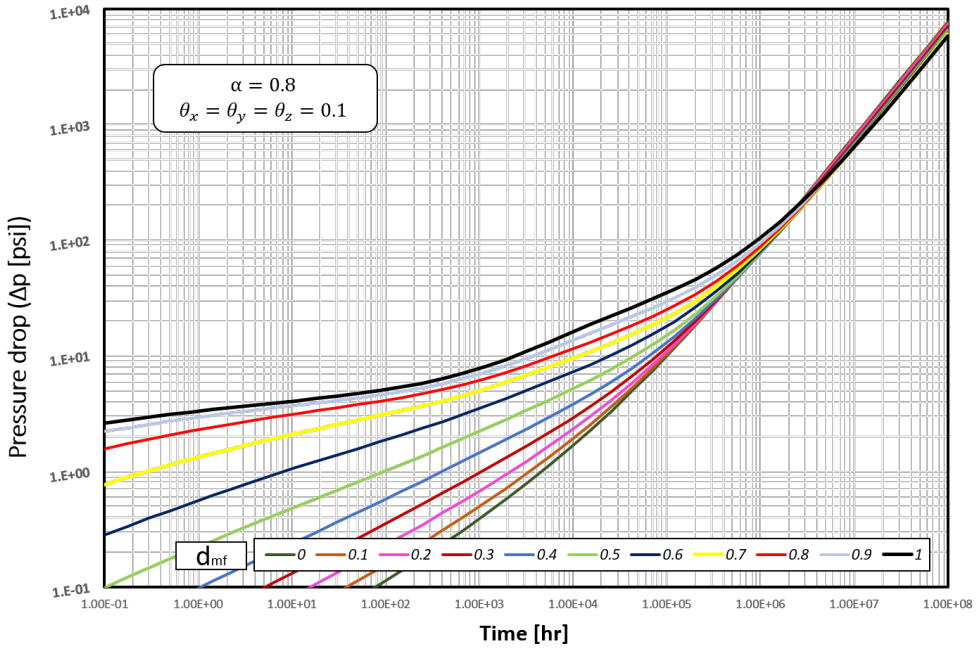

Figure 7.2: Pressure sensitivity: fractal dimension, dmf

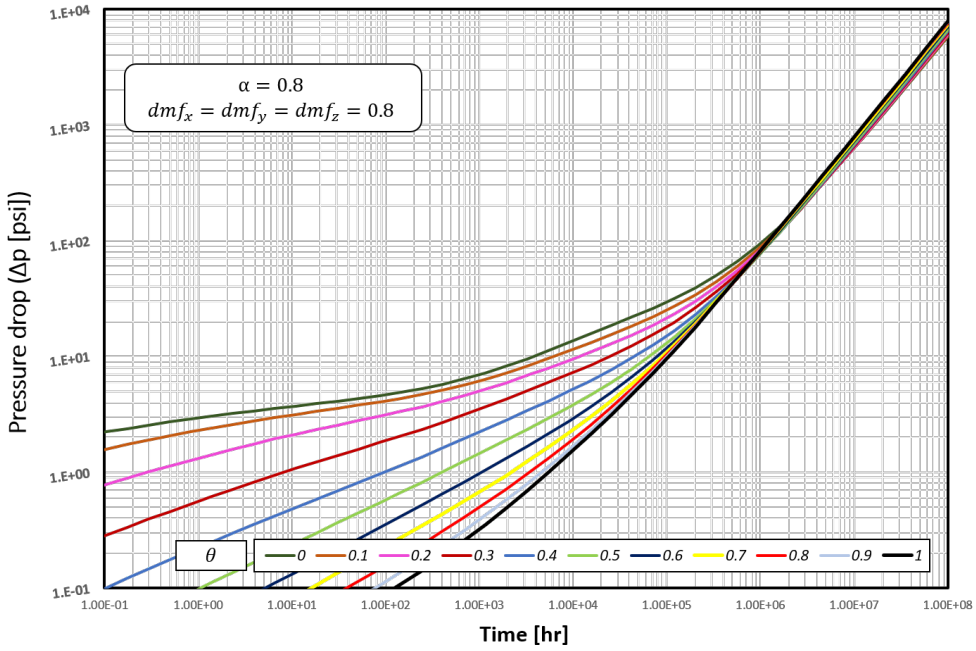

Figure 7.3: Pressure sensitivity: connectivity index, θ

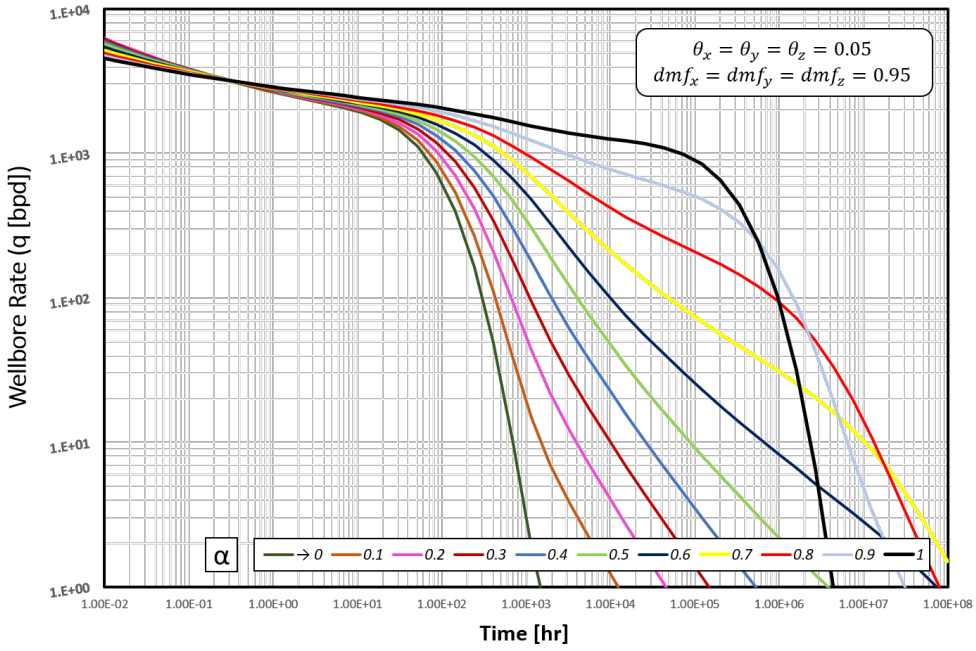

Figure 7.4: Rate response sensitivity: anomalous diffusion exponent, α

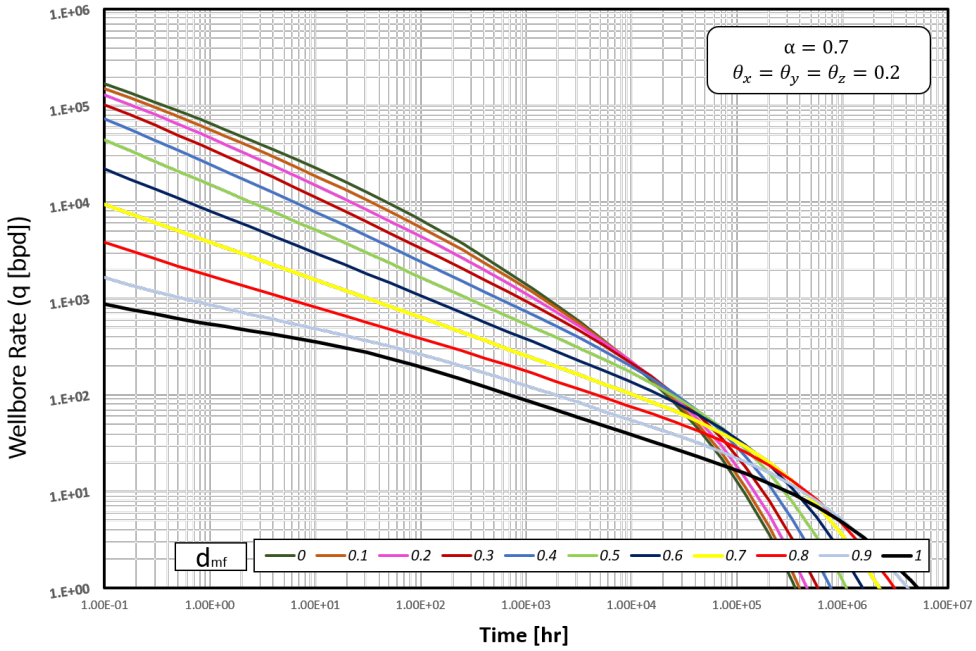

Figure 7.5: Rate response sensitivity: fractal dimension, dmf

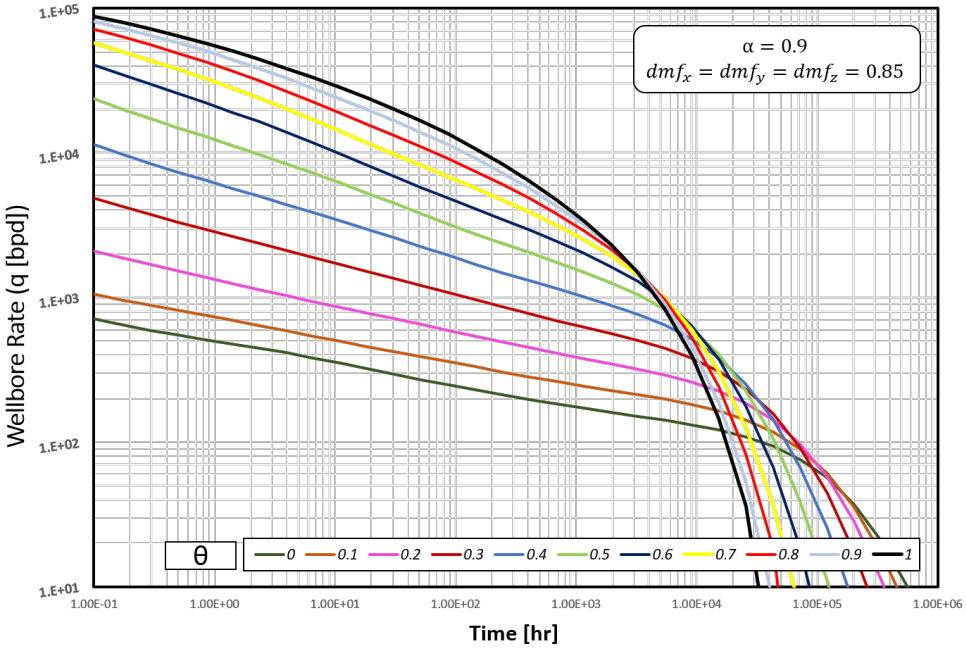

Figure 7.6: Rate response sensitivity: fractal dimension, dmf

Chapter 8

Conclusions and Recommendations

Unconventional reservoirs exhibit new challenges for modeling fluid flow, many of which are scale-dependent. The aim of this research was to combine the application of two novel approaches (fractal theory and anomalous diffusion), for modeling multidimensional flow in fractured media. The results of this work allowed to establish the following conclusions.

- A numerical multidimensional-flow model was developed to describe anomalous diffusive flow, of a single-phase fluid, on an unconventional reservoir having fractal characteristics. The pseudo-steady state contribution of matrix blocks was considered explicitly.
- Results show that the typical slopes are not recovered when fractal characteristics and anomalous diffusion are present.
- Production from highly fractured examples was considerably higher than those where stimulation reaches only the propped section. Attention should be pay on designing fracture treatments capable of creating fracture networks beyond the propped sections.
- Creating connectivity of the induced and preexisting fractures must be set as a goal for fracture treatments; results show that the rate differences between highly and poorly connected media reaches orders of magnitude.

Finally, some recommendations for future works are presented next.

- To include multiphase-flow in three dimensions such as the model presented by Holy (2016) for one-dimensional flow.
- To develop an anlytical solution for anomalous diffusion gas flow for considering cartesian coordinates, such as the one developed by Amin et al. (2017), for radial coordinates.
- To analyze different real cases with discrete numerical models, using an optimization algorithm to obtain the values of the parameters that are involved in the solution.
- At the time this work is presented, these formulations are not included as part of comercial softwares. New tools including these effects should be developed.

Nomenclature

$\hat{q}$	Flux per unit of rock volume between two regions
ct	Total compressibility
H	Simulated thickness
k	Permeability
k_α	Permeability at α
L	Length
n	Time level
P	Finite difference approximation to pressure
p	Pressure
q	Rate
t	Time
V_r	Rock volume
W	Width
x	Position in x-direction
y	Position in y-direction
z	Position in z-direction
B	Transmissibility in $j - \frac{1}{2}$

C central coefficient

F Transmissibility in $j + \frac{1}{2}$

N Transmissibility in $k + \frac{1}{2}$

S Transmissibility in $k - \frac{1}{2}$

Greek

α Anomalous diffusion exponent and derivation order

Δ Delta operator

Γ Gamma function

γ Function of the derivation order

μ Viscosity

ω Function of time steps

ϕ Porosity

τ Integration variable

θ Connectivity index

Subscripts

b Permability fractal scaling exponent

c Porosity and Matrix block size fractal scaling exponent

F Hydraulic fractures

f Natural fractures

i Grid-division in x-direction

j Grid-division in y-direction

k Grid-division in z-direction

m Matrix elements

max Last division

s Stimulation

v Unstimulated, original, virgin

w Well

References

[1] Acuña, J. A. and Y. C. Yortsos

1995. Application of fractal geometry to the study of networks of fractures and their pressure transient. *Water Resources Research*, 31(3):527–540.

[2] Agrawal, S., M. M. Sharma, et al.

2020. Mechanisms for the Creation of a Stimulated Rock Volume Around Hydraulic Fractures. In *54th US Rock Mechanics/Geomechanics Symposium*. American Rock Mechanics Association.

[3] Albinali, A.

2016. *Analytical solution for anomalous diffusion in fractured nano-porous reservoirs*. PhD thesis, Colorado School of Mines.

[4] Amin, M. E., R. Ahmed, and S. Shuyu

2017. Analytical solution for fractional derivative gas-flow equation in porous media. *Results in Physics*, 7:2432–2438.

[5] Angstmann, C. N., I. C. Donnelly, and B. I. Henry

2013. Continuous Time Random Walks with Reactions Forcing and Trapping. *Mathematical Modelling of Natural Phenomena*, 8(2):17–27.

[6] Camacho-Velázquez, R., G. Fuentes-Cruz, and M. A. Vasquez-Cruz

2008. Decline-Curve Analysis of Fractured Reservoirs with Fractal Geometry. *SPE Reservoir Evaluation & Engineering*, 11(03):606–619.

[7] Caputo, M.

1967. Linear models of dissipation whose Q is almost frequency independent—II. *Geophysical Journal International*, 13(5):529–539.

[8] Chang, J. and Y. C. Yortsos

1990. Pressure transient analysis of fractal reservoirs. *SPE Formation Evaluation*, 5(01):31–38.

[9] Chen, C. and R. Raghavan
2015. Transient flow in a linear reservoir for space–time fractional diffusion. *Journal of Petroleum Science and Engineering*, 128:194–202.

[10] Chu, W., N. Pandya, R. W. Flumerfelt, and C. Chen
2017. Rate-Transient Analysis Based on Power-Law Behavior for Permian Wells. In *Day 3 Wed, October 11, 2017*. SPE.

[11] Chu, W., K. Scott, R. Flumerfelt, and C.-C. Chen
2018. A New Technique for Quantifying Pressure Interference in Fractured Horizontal Shale Wells. In *Day 2 Tue, September 25, 2018*. SPE.

[12] Cossio Santizo, M.
2012. *A Semi-Analytic Solution for Flow in Finite-Conductivity Vertical Fractures Using Fractal Theory*. PhD thesis.

[13] Daniels, J. L., G. A. Waters, J. H. Le Calvez, D. Bentley, J. T. Lassek, et al.
2007. Contacting more of the barnett shale through an integration of real-time microseismic monitoring, petrophysics, and hydraulic fracture design. In *SPE annual technical conference and exhibition SPE-110562-MS*. Society of Petroleum Engineers.

[14] de Swaan O., A.
1976. Analytic Solutions for Determining Naturally Fractured Reservoir Properties by Well Testing. *Society of Petroleum Engineers Journal*, 16(03):117–122.

[15] Fisher, M. K., C. A. Wright, B. M. Davidson, N. P. Steinsberger, W. S. Buckler, A. Goodwin, and E. O. Fielder
2005. Integrating fracture mapping technologies to improve stimulations in the Barnett shale. *SPE Production & Facilities*, 20(02):85–93.

[16] Flamenco-Lopez, F. and R. Camacho-Velázquez
2003. Determination of fractal parameters of fracture networks using pressure-transient data. *SPE Reservoir Evaluation & Engineering*, 6(01):39–47.

[17] Fomin, S.
2011. MATHEMATICAL MODELING OF ANOMALOUS DIFFUSION IN POROUS MEDIA. *Fractional Differential Calculus*, Volume 1,:1–28.

[18] Fuentes-Cruz, G., E. Gildin, and P. P. Valkó
2014. Analyzing production data from hydraulically fractured wells: the concept of induced permeability field. *SPE Reservoir evaluation & engineering*, 17(02):220–232.

[19] Gale, J. F. W., S. E. Laubach, J. E. Olson, P. Eichhubl, and A. Fall
2014. Natural fractures in shale: A review and new observations of Natural Fractures in Shale. *AAPG bulletin*, 98(11):2165–2216.

[20] Gillespie, D. T. and E. Seitaridou
2012. *Simple Brownian Diffusion*. Oxford University Press.

[21] Hardy, H. H. and R. A. Beier
1994. *Fractals in reservoir engineering*. World Scientific.

[22] Henry, B. I., T. A. M. Langlands, and P. Straka
2010. An Introduction to Fractional Diffusion. In *Complex Physical, Biophysical and Econophysical Systems*. WORLD SCIENTIFIC.

[23] Holy, R. and E. Ozkan
2017. Numerical Modeling of 1-D Anomalous Diffusion in Unconventional Wells Using a Non-Uniform Mesh. In *Proceedings of the 5th Unconventional Resources Technology Conference 2017*. American Association of Petroleum Geologists.

[24] Holy, R. W.
2016. *Numerical investigation of 1D anomalous diffusion in fractured nanoporous reservoirs*. PhD thesis, Colorado School of Mines.

[25] Javadpour, F. et al.
2009. Nanopores and apparent permeability of gas flow in mudrocks (shales and siltstone). *Journal of Canadian Petroleum Technology*, 48(08):16–21.

[26] Kazemi, H.
1969. Pressure Transient Analysis of Naturally Fractured Reservoirs with Uniform Fracture Distribution. *Society of Petroleum Engineers Journal*, 9(04):451–462.

[27] Mandelbrot, B. B.
1989. Fractal geometry: what is it, and what does it do? *Proceedings of the Royal Society of London. A. Mathematical and Physical Sciences*, 423(1864):3–16.

[28] Maxwell, S. C., T. I. Urbancic, N. Steinsberger, R. Zinno, et al.
2002. Microseismic imaging of hydraulic fracture complexity in the Barnett shale. In *SPE annual technical conference and exhibition*. Society of Petroleum Engineers.

[29] Metzler, R. and J. Klafter
2000. The random walk's guide to anomalous diffusion: a fractional dynamics approach. *Physics reports*, 339(1):1–77.

[30] Murio, D. A.
2008. Implicit finite difference approximation for time fractional diffusion equations. *Computers & Mathematics with Applications*, 56(4):1138–1145.

[31] Narasimhan, T. N.
2009. The dichotomous history of diffusion. *Physics Today*, 62(7):48–53.

[32] O'Shaughnessy, B. and I. Procaccia
1985. Analytical solutions for diffusion on fractal objects. *Physical review letters*, 54(5):455.

[33] Ozcan, O.
2014. Fractional diffusion in naturally fractured unconventional reservoirs. Master's thesis, Colorado School of Mines.

[34] Raghavan, R.
2011. Fractional derivatives: Application to transient flow. *Journal of Petroleum Science and Engineering*, 80(1):7–13.

[35] Raghavan, R. and C. Chen
2013. Fractional diffusion in rocks produced by horizontal wells with multiple, transverse hydraulic fractures of finite conductivity. *Journal of Petroleum Science and Engineering*, 109:133–143.

[36] Raghavan, R. and C. Chen
2016. Rate Decline, Power Laws, and Subdiffusion in Fractured Rocks. *SPE Reservoir Evaluation & Engineering*, 20(03):738–751.

[37] Raghavan, R. and C.-C. Chen
2018. A Conceptual Structure to Evaluate Wells Producing Fractured Rocks of the Permian Basin. In *Day 2 Tue, September 25, 2018*. SPE.

[38] Raghavan, R. and C.-C. Chen
2019. Evaluation of Fractured Rocks through Anomalous Diffusion. In *Day 4 Fri, April 26, 2019*. SPE.

[39] Sokolov, I. M. and J. Klafter
2005. From diffusion to anomalous diffusion: A century after Einstein's Brownian motion. *Chaos: An Interdisciplinary Journal of Nonlinear Science*, 15(2):026103.

[40] Turner, J.
2012. Brownian Motion Applied to Human Intersections. Master's thesis, Texas State University-San Marcos.

[41] Vlahos, L., H. Isliker, Y. Kominis, and K. Hizanidis
2008. Normal and Anomalous Diffusion: A Tutorial.

[42] Wang, W., Y. Su, Z. Zhou, G. Sheng, R. Zhou, M. Tang, X. Du, J. An, et al.
2017. Method of characterization of complex fracture network with combination of microseismic using fractal theory. In *SPE/IATMI Asia Pacific oil & gas conference and exhibition*. Society of Petroleum Engineers.

[43] Webster, J.
2014. GOING GLOBAL: TIGHT OILPRODUCTION . *IHS Markit*.

[44] Wu, W.
2017. Unpropped fractures in shale : surface topography, mechanical properties and hydraulic conductivity. Master's thesis, The University of Texas at Austin.

[45] Xu, W., J. H. Le Calvez, M. J. Thiercelin, et al.
2009. Characterization of hydraulically-induced fracture network using treatment and microseismic data in a tight-gas sand formation: a geomechanical approach. In *SPE tight gas completions conference*. Society of Petroleum Engineers.

[46] Yucel Akkutlu, I. and E. Fathi
2012. Multiscale gas transport in shales with local kerogen heterogeneities. *SPE journal*, 17(04):1002–1011.

Appendix A

Model derivation

Consider a horizontal well with a set of multiple identical hydraulic fractures (see **figure A.1**).

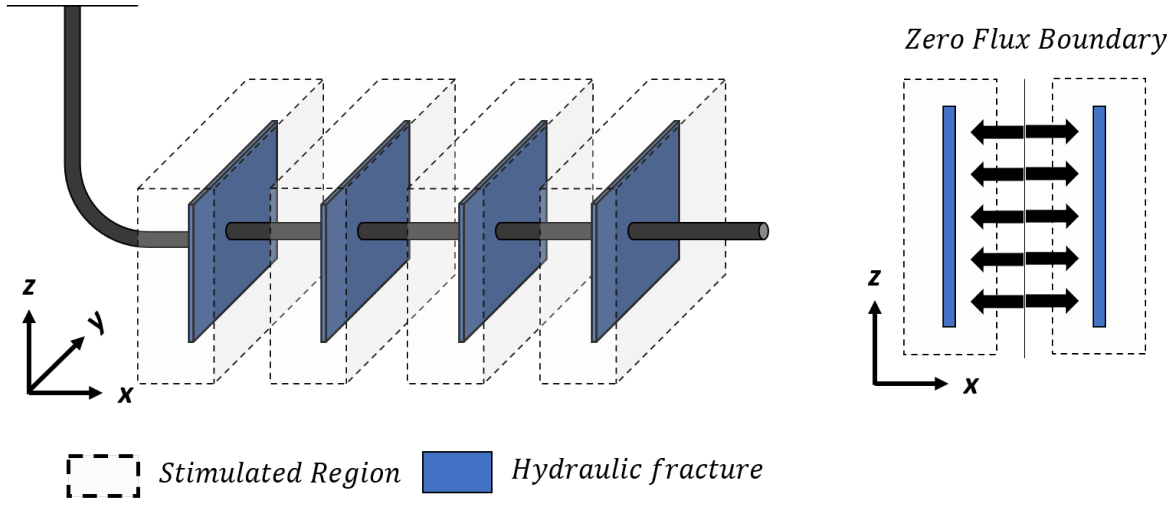

Figure A.1: Horizontal symmetrically fractured well

Symmetry of the fractures was assumed and only one-eight of the drainage area was considered. Computational time is reduced through this consideration. The domain is subdivided into three main regions: hydraulic fracture, SRV, and undisturbed region (see **figure A.2**).

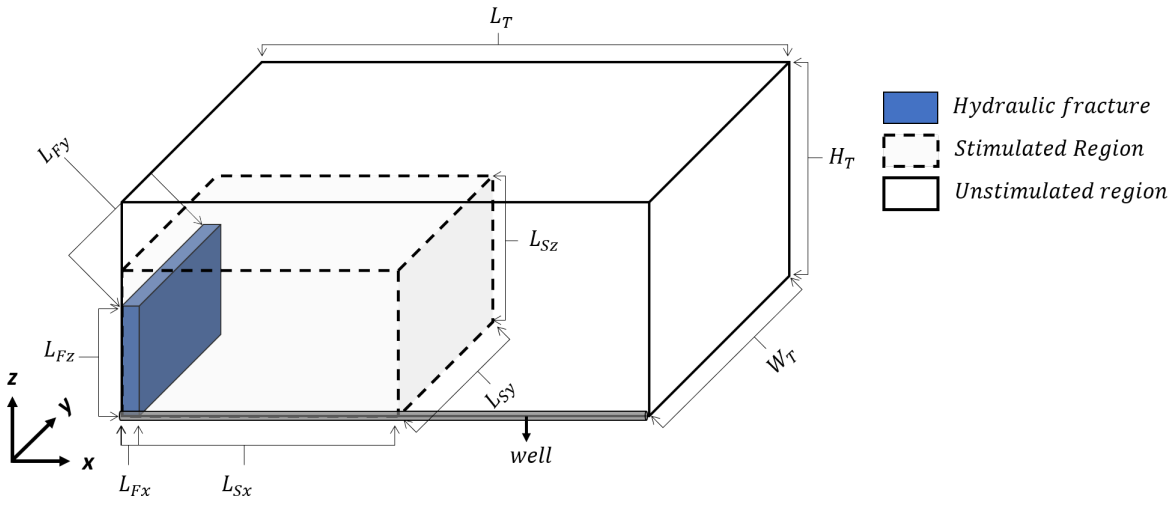

Figure A.2: Three regions under consideration

The continuous flow equations for each region are approximated through a finite difference scheme. A logarithmic mesh, both for time and space, is employed. Central and backward difference approximations are used for space and time respectively (**figure A.3**).

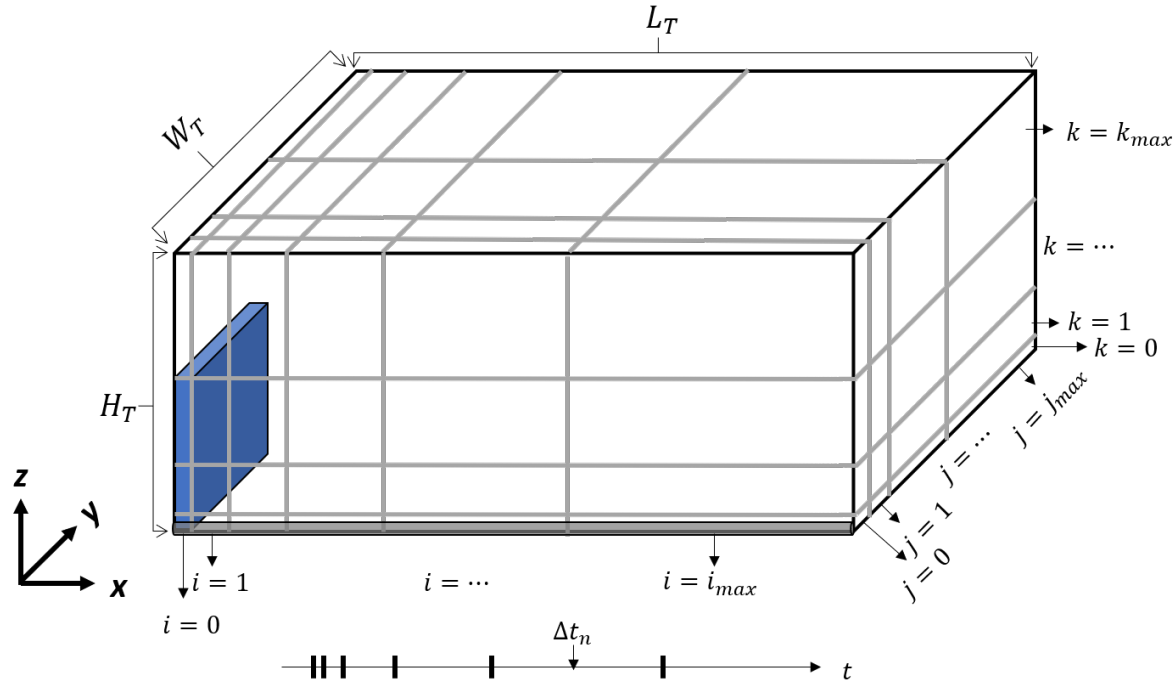

Figure A.3: Logarithmic mesh

The subscripts required for finite difference derivations are shown below (see **figure A.4**)

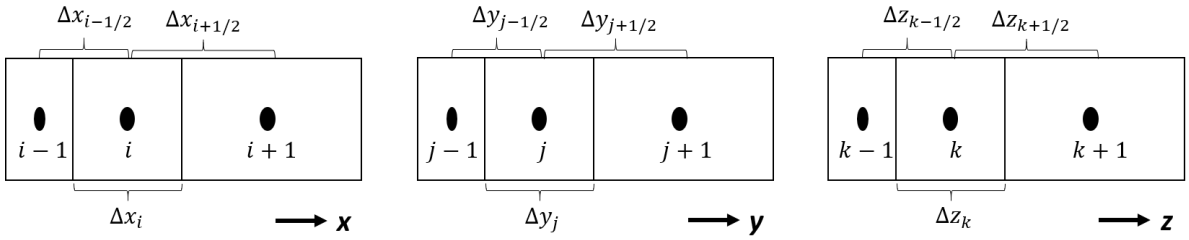

Figure A.4: Grid cell nomenclature

A.1 Hydraulic Fracture

A propped hydraulic fracture with homogeneous and isotropic properties is considered. Normal diffusion governs fluid flow in this region, and thus, conventional Darcy's law is introduced to continuity equation. The governing equation is given as

$$\frac{\partial}{\partial y}\left[\frac{k_F}{\mu}\frac{\partial p_F}{\partial y}\right]+\frac{\partial}{\partial z}\left[\frac{k_F}{\mu}\frac{\partial p_F}{\partial z}\right]=(\phi ct)_F\frac{\partial p_F}{\partial t} \tag{A.1}$$

$$for\ 0>x<w_f/2,\ 0>y<L_{Fy},\ 0>z<L_{Fz},$$

where $w_F/2$, L_{Fy} and L_{Fz} represent the hydraulic fracture lenghts in the corresponding directions.

Boundary conditions are schematized in A.5

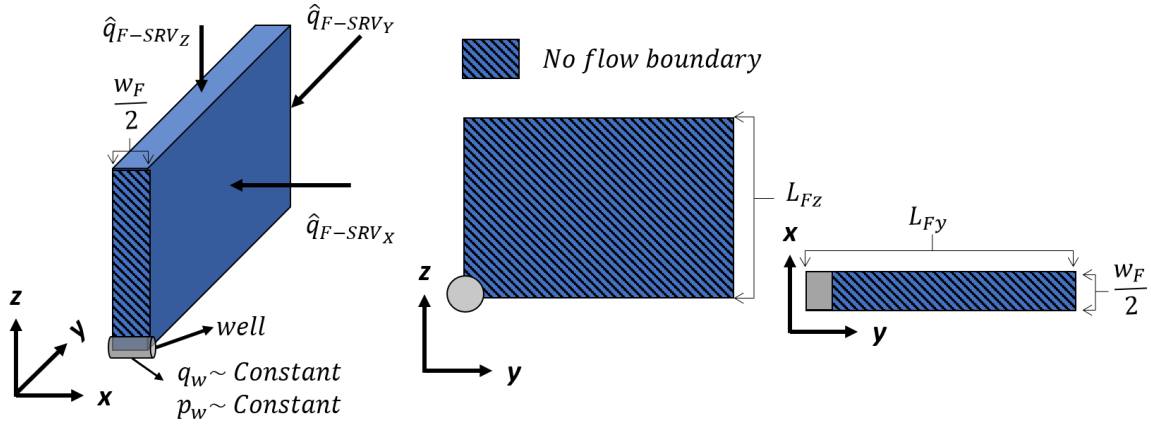

Figure A.5: Hydraulic fracture boundary conditions

The conditions to be satisfied at the boundaries between hydraulic fracture and SRV are represented through $\hat{q}_{F-SRV_x}$, $\hat{q}_{F-SRV_y}$, $\hat{q}_{F-SRV_z}$ in figure A.5. These terms are defined as

$$\hat{q}_{F-SRV_x}\Big|_{x=w_F/2} = -\frac{k_{(\alpha,b)_x}}{\mu}\frac{\partial^{1-\alpha}}{\partial t^{1-\alpha}}\left(\frac{\partial p}{\partial x}\right)\Big|_{x=w_F/2} \tag{A.2}$$

$$\hat{q}_{F-SRV_y}\Big|_{L_{F_y}} = -\frac{k_{(\alpha,b)_y}}{\mu}\frac{\partial^{1-\alpha}}{\partial t}\left(\frac{\partial p}{\partial y}\right)\Big|_{L_{F_y}} \tag{A.3}$$

$$\hat{q}_{F-SRV_z}\Big|_{L_{F_z}} = -\frac{k_{(\alpha,b)_z}}{\mu}\frac{\partial^{1-\alpha}}{\partial t}\left(\frac{\partial p}{\partial z}\right)\Big|_{L_{F_z}} \tag{A.4}$$

Fluids reach the wellbore only via hydraulic fracture. The boundary at the wellbore will be considered next (Constant bottomhole pressure or constant rate). The constant 8, in the left side of equation A.5, arises because only one-eight of the hydraulic fracture is being modeled.

$$\frac{\hat{q_{w/F}}}{8}(x=0,y=0,z=0,t) = \frac{k_{Fav}}{\mu}\frac{\partial p}{\partial x}\Big|_{(0,0,0)} \tag{A.5}$$

$q_{w/F}$ represents the contribution of each symmetric HF, to the total wellbore rate.

Problem's symmetry inhibits fluids to cross the planes bisecting hydraulic fracture in any of the three directions (again, note that only one-eight of the system is modeled). These no-flow boundary conditions are given by

$$\frac{\partial P_F}{\partial x}\Big|_{x=0} = 0 \tag{A.6}$$

$$\frac{\partial P_F}{\partial y}\Big|_{y=0} = 0 \tag{A.7}$$

$$\frac{\partial P_F}{\partial z}\Big|_{z=0} = 0 \tag{A.8}$$

A.1.1 Finite difference approximation

For the grid cell at (i, j, k) which belongs to the hydraulic fracture domain, the finite difference approximation of equation A.1 is given by

$$\frac{1}{\Delta y_j}\left[\left(\frac{k_F}{\mu}\right)_{j+\frac{1}{2}}\frac{P_{F_{j+1}}^{n+1}-P_{F_j}^{n+1}}{\Delta y_{j+1/2}}-\left(\frac{k_F}{\mu}\right)_{j-\frac{1}{2}}\frac{P_{F_j}^{n+1}-P_{F_{j-1}}^{n+1}}{\Delta y_{j-1/2}}\right]+$$

$$\frac{1}{\Delta z_j}\left[\left(\frac{k_F}{\mu}\right)_{k+\frac{1}{2}}\frac{P_{F_{k+1}}^{n+1}-P_{F_k}^{n+1}}{\Delta z_{j-1/2}}-\left(\frac{k_F}{\mu}\right)_{k-\frac{1}{2}}\frac{P_{F_k}^{n+1}-P_{F_{k-1}}^{n+1}}{\Delta z_{j-1/2}}\right]+$$

$$=(\phi ct)_{Fj,k}\frac{P_{F_{j,k}}^{n+1}-P_{F_{j,k}}^{n}}{\Delta t^n}. \quad \text{(A.9)}$$

The rock volume ($Vr_{i,j,k}$) for each grid cell is defined as

$$Vr_{i,j,k}=\Delta x_i\times\Delta y_j\times\Delta z_k \quad \text{(A.10)}$$

All hydraulic fracture cells are contained within the first grid division of $\boldsymbol{x}$ direction. This division has a size of one-half the hydraulic fracture width, then $\Delta x_0 = w_F/2$.

Multiplying equation A.9 by rock volume and rearranging the equation

$$\left[\frac{w_F/2\ \Delta z_k}{\Delta y_{j+\frac{1}{2}}}\left(\frac{k_F}{\mu}\right)_{j+1/2}\right]P_{F_{j+1}}^{n+1}\left[\frac{w_F/2\ \Delta y_j}{\Delta z_{k+\frac{1}{2}}}\left(\frac{k_F}{\mu}\right)_{k+1/2}\right]P_{F_{k+1}}^{n+1}-\left[\frac{w_F/2\ \Delta z_k}{\Delta y_{j+\frac{1}{2}}}\left(\frac{k_F}{\mu}\right)_{j+1/2}+\right.$$

$$\left.\frac{w_F/2\ \Delta y_j}{\Delta z_{k+\frac{1}{2}}}\left(\frac{k_F}{\mu}\right)_{k+1/2}+\frac{w_F/2\ \Delta z_k}{\Delta y_{j-\frac{1}{2}}}\left(\frac{k_F}{\mu}\right)_{j-1/2}+\frac{w_F/2\ \Delta y_j}{\Delta z_{k-\frac{1}{2}}}\left(\frac{k_F}{\mu}\right)_{k-1/2}+\frac{(\phi ct)_{Fj,k}}{\Delta t^n}\right]P_{F_{j,k}}^{n+1}$$

$$\left[\frac{w_F/2\ \Delta z_k}{\Delta y_{j-\frac{1}{2}}}\left(\frac{k_F}{\mu}\right)_{j-1/2}\right]P_{F_{j-1}}^{n+1}+\left[\frac{w_F/2\ \Delta y_j}{\Delta z_{k-\frac{1}{2}}}\left(\frac{k_F}{\mu}\right)_{k-1/2}\right]P_{F_{k-1}}^{n+1}=-\frac{(\phi ct)_{Fj,k}}{\Delta t^n}\ P_{F_{j,k}}^{n}\ . \quad \text{(A.11)}$$

Transmissibility coefficients are defined as follows,

$$F_{Fj,k} = \left[\frac{w_F/2\ \Delta z_k}{\Delta y_{j+\frac{1}{2}}} \left(\frac{k_F}{\mu} \right)_{j+1/2} \right] \tag{A.12}$$

$$B_{Fj,k} = \left[\frac{w_F/2\ \Delta z_k}{\Delta y_{j-\frac{1}{2}}} \left(\frac{k_F}{\mu} \right)_{j-1/2} \right] \tag{A.13}$$

$$N_{Fj,k} = \left[\frac{w_F/2\ \Delta y_j}{\Delta z_{k+\frac{1}{2}}} \left(\frac{k_F}{\mu} \right)_{k+1/2} \right] \tag{A.14}$$

$$S_{Fj,k} = \left[\frac{w_F/2\ \Delta y_j}{\Delta z_{k-\frac{1}{2}}} \left(\frac{k_F}{\mu} \right)_{k-1/2} \right]. \tag{A.15}$$

For convinience, letters are selected to represent North ($k+\frac{1}{2}$), South ($k-\frac{1}{2}$), Forward ($j+\frac{1}{2}$) and Backward ($j-\frac{1}{2}$) directions. Equation A.11 can be written in a compact form as

$$N_{Fj,k}\ P_{F_{k+1}}^{n+1} \ +\ F_{Fj,k}\ P_{F_{j+1}}^{n+1} \ +\ C_{Fj,k}\ P_{F_{i,j}}^{n+1} \ +\ S_{Fj,k}\ P_{F_{k-1}}^{n+1} + \ B_{Fj,k}\ P_{F_{j-1}}^{n+1} \ = R_{Fi,j} \tag{A.16}$$

where

$$C_{i,j} \ = - \ \left[N_{Fj,k} \ +\ S_{Fj,k} \ +\ F_{Fj,k} \ +\ B_{Fj,k} \right] \tag{A.17}$$

$$R_{Fi,j} = - \ \frac{(\phi ct)_{Fj,k}}{\Delta t^n} \ P_{F_{j,k}}^{n} \ . \tag{A.18}$$

Equation A.16 represents the recurrence equation for any node within the hydraulic fracture. Those grid cells located at the boundary with SRV must also consider the corresponding additional terms $\hat{q}_{F-SRV_x}$,
$hat q_{F-SRV_y}$, $\hat{q}_{F-SRV_z}$. The finite-difference approximation of the time-fractional derivative can be found in Appendix B (Note that these terms are anomalous diffusion governed).

$$\hat{q}_{F-SRV_x} = -\frac{k_{\alpha,b_x}}{\mu}\ \sigma_\alpha \sum_{k=1}^{n+1} \omega_k^\alpha \left[\frac{\partial p\,(x,t_k)}{\partial x} - \frac{\partial p\,(x,t_{k-1})}{\partial x} \right] \tag{A.19}$$

$$\hat{q}_{F-SRV_y} = -\frac{k_{\alpha,b_y}}{\mu}\ \sigma_\alpha \sum_{k=1}^{n+1} \omega_k^\alpha \left[\frac{\partial p\,(y,t_k)}{\partial y} - \frac{\partial p\,(y,t_{k-1})}{\partial y} \right] \tag{A.20}$$

$$\hat{q}_{F-SRV_z} = -\frac{k_{\alpha,b_z}}{\mu}\ \sigma_\alpha \sum_{k=1}^{n+1} \omega_k^\alpha \left[\frac{\partial p\,(z,t_k)}{\partial z} - \frac{\partial p\,(x,t_{k-1})}{\partial x} \right]. \tag{A.21}$$

Now the pressure gradient inside previous equations is approximated through a forward difference. For simplicity only the equation A.19 is presented, identical procedure should be followed for equation A.20 and A.21.

$$[\hat{q}_{F-SRV_x}]^{n+1} = -\frac{k_{\alpha,b_x}}{\mu}\ \sigma_\alpha \sum_{k=1}^{n+1} \omega_k^\alpha \left[\frac{P_{SRV}^k - P_F^k}{\Delta x_{i+1/2}} - \frac{P_{SRV}^{k-1} - P_F^{k-1}}{\Delta x_{i+1/2}}\right]. \tag{A.22}$$

Note that this equation is derived for the time level $n+1$; variables for previous time step ($Tstep = 0, 1, 2, ..., n$) have already been solved. Separating known from unknown variables, equation A.22 results in

$$[\hat{q}_{F-SRV_x}]^{n+1} = -\frac{k_{\alpha,b_x}\ \sigma_\alpha}{\mu}\ \left[\omega_{n+1}^\alpha \left[\frac{P_{SRV}^{n+1} - P_F^{n+1}}{\Delta x_{i+1/2}} - \frac{P_{SRV}^{n} - P_F^{n}}{\Delta x_{i+1/2}}\right]\right]$$

$$- \frac{k_{\alpha,b_x}\ \sigma_\alpha}{\mu}\ \sum_{k=1}^{n} \omega_k^\alpha \left[\frac{P_{SRV}^k - P_F^k}{\Delta x_{i+1/2}} - \frac{P_{SRV}^{k-1} - P_F^{k-1}}{\Delta x_{i+1/2}}\right] \tag{A.23}$$

Finally the finite-difference approximation to the fractional flux law is given by

$$[\hat{q}_{F-SRV_x}]^{n+1} = -\frac{k_{\alpha,b_x}\ \sigma_\alpha}{\mu\ \Delta x_{i+1/2}}\ \omega_{n+1}^\alpha \left[P_{SRV}^{n+1} - P_F^{n+1}\right] - \frac{k_{\alpha,b_x}\ \sigma_\alpha}{\mu\ \Delta x_{i+1/2}} \omega_{n+1}^\alpha \left[-P_{SRV}^{n} + P_F^{n}\right]$$

$$- \frac{k_{\alpha,b_x}\ \sigma_\alpha}{\mu\ \Delta x_{i+1/2}}\ \sum_{k=1}^{n} \omega_k^\alpha \left[P_{SRV}^k - P_F^k - P_{SRV}^{k-1} + P_F^{k-1}\right] \tag{A.24}$$

A.2 Region Outside the Hydraulic Fracture

Two sections conform this region, the Stimulated Reservoir Volume (SRV), and the Outside Reservoir (OR). In general, the same equation governs flow in both regions. The only difference lies in porosity, phenomenological flow coefficient (permeability at $\boldsymbol{\alpha}$), and matrix block size distribution. Uniform properties are considered for the outside region (stimulation is negligible far away from the main fracture plane), and power-law decline distribution is considered inside the SRV.

A.2.1 Distribution of properties

Consider the stimulated region delimited by $L_{S_x}, L_{S_y}, L_{S_z}$. Following a fractal approach, power-law relationships are used to model the decline in porosity ϕ_c, phenomenological flow

coefficient (permeability at α) $k_{\alpha,b}$, and matrix block size $\left(L_{c_x}, L_{c_y}, L_{c_z}\right)$. Note that properties inside the hydraulic fracture are left behind (ϕ_F, k_F). Original reservoir properties are found outside from this region $(\phi_v, k_{\alpha,v_x}, k_{\alpha,v_y}, k_{\alpha,v_z}, L_{c_x}, L_{c_y}, L_{c_z})$. Note also that stimulation magnitude decreases from point A to B (See figure A.6) and that subscript c makes reference to the fractal exponent c.

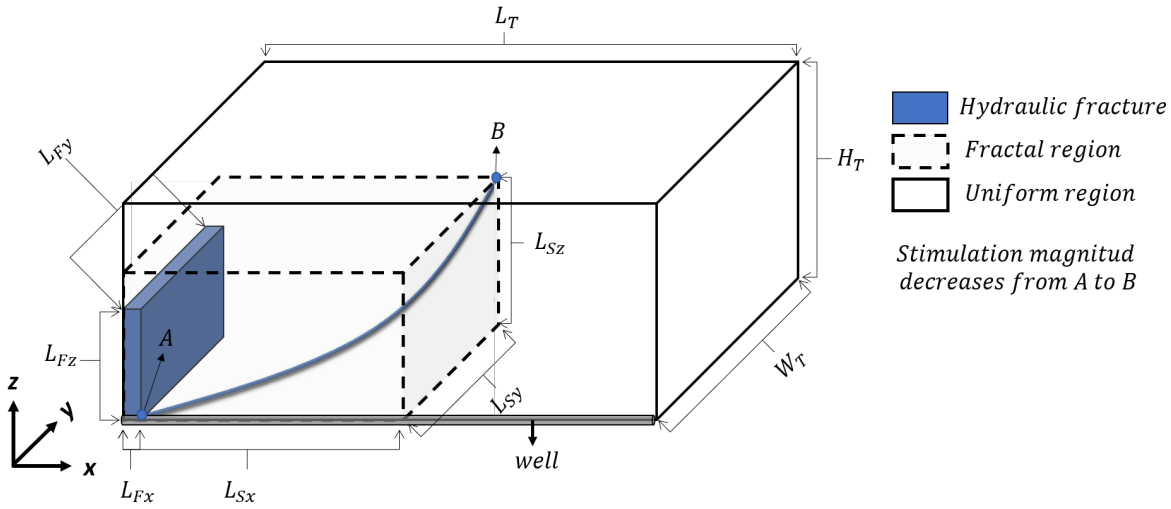

Figure A.6: Schematization of stimulation magnitud at SRV

The three properties are assigned with the following definitions:

- Phenomenological Flow Coefficient (permeability at α)

$$k_{\alpha,b_x} = \begin{cases} k_{\alpha,v_x}\left[\left(\frac{x}{L_{S_x}}\right)^{b_x}\left(\frac{y}{L_{S_y}}\right)^{b_y}\left(\frac{z}{L_{S_z}}\right)^{b_z}\right] & \text{for } x \le L_{S_x},\ y \le L_{S_y},\ z \le L_{S_z} \\ k_{\alpha,v_x} & \text{for } x > L_{S_x},\ y > L_{S_y},\ z > L_{S_z} \end{cases} \tag{A.25}$$

$$k_{\alpha,b_y} = \begin{cases} k_{\alpha,v_y}\left[\left(\frac{x}{L_{S_x}}\right)^{b_x}\left(\frac{y}{L_{S_y}}\right)^{b_y}\left(\frac{z}{L_{S_z}}\right)^{b_z}\right] & \text{for } x \le L_{S_x},\ y \le L_{S_y},\ z \le L_{S_z} \\ k_{\alpha,v_y} & \text{for } x > L_{S_x},\ y > L_{S_y},\ z > L_{S_z} \end{cases} \tag{A.26}$$

$$k_{\alpha,b_z} = \begin{cases} k_{\alpha,v_z}\left[\left(\frac{x}{L_{S_x}}\right)^{b_x}\left(\frac{y}{L_{S_y}}\right)^{b_y}\left(\frac{z}{L_{S_z}}\right)^{b_z}\right] & \text{for } x \le L_{S_x},\ y \le L_{S_y},\ z \le L_{S_z} \\ k_{\alpha,v_z} & \text{for } x > L_{S_x},\ y > L_{S_y},\ z > L_{S_z} \end{cases} \tag{A.27}$$

where

$$b_x = dmf_x - \theta_x - 1 \tag{A.28}$$

$$b_y = dmf_y - \theta_y - 1 \tag{A.29}$$

$$b_z = dmf_z - \theta_z - 1 \tag{A.30}$$

- Porosity

$$\phi_c = \begin{cases} \phi_v \left[\left(\frac{x}{L_{S_x}} \right)^{c_x} \left(\frac{y}{L_{S_y}} \right)^{c_y} \left(\frac{z}{L_{S_z}} \right)^{c_z} \right] & \text{for } x \le L_{S_x},\ y \le L_{S_y},\ z \le L_{S_z} \\ \phi_v & \text{for } x > L_{S_x},\ y > L_{S_y},\ z > L_{S_z} \end{cases} \tag{A.31}$$

where

$$c_x = dmf_x - 1 \tag{A.32}$$

$$c_y = dmf_y - 1 \tag{A.33}$$

$$c_z = dmf_z - 1 \tag{A.34}$$

- Matrix block size

$$L_x = \begin{cases} L_{v_x} \left[\left(\frac{L_{S_x}}{x} \right)^{c_x} \left(\frac{L_{S_y}}{y} \right)^{c_y} \left(\frac{L_{S_z}}{z} \right)^{c_z} \right] & \text{for } x \le L_{S_x},\ y \le L_{S_y},\ z \le L_{S_z} \\ L_{v_x} & \text{for } x > L_{S_x},\ y > L_{S_y},\ z > L_{S_z} \end{cases} \tag{A.35}$$

$$L_y = \begin{cases} L_{v_y} \left[\left(\frac{L_{S_x}}{x} \right)^{c_x} \left(\frac{L_{S_y}}{y} \right)^{c_y} \left(\frac{L_{S_z}}{z} \right)^{c_z} \right] & \text{for } x \le L_{S_x},\ y \le L_{S_y},\ z \le L_{S_z} \\ L_{v_y} & \text{for } x > L_{S_x},\ y > L_{S_y},\ z > L_{S_z} \end{cases} \tag{A.36}$$

$$L_z = \begin{cases} L_{v_z} \left[\left(\frac{L_{S_x}}{x} \right)^{c_x} \left(\frac{L_{S_y}}{y} \right)^{c_y} \left(\frac{L_{S_z}}{z} \right)^{c_z} \right] & \text{for } x \le L_{S_x},\ y \le L_{S_y},\ z \le L_{S_z} \\ L_{v_z} & \text{for } x > L_{S_x},\ y > L_{S_y},\ z > L_{S_z} \end{cases} \tag{A.37}$$

Note that matrix block size should increase with distance from the main fracture plane.

A.2.2 Governing Equation

As previously stated, flow in both regions (SRV and OR) is governed by the same anomalous diffusion equation. However, some flow improvements occur inside the SRV. These flow improvements are captured by assigning the properties of the medium through power-law relationships.

The anomalous flux law is introduced into the continuity equation. Flow in three directions is considered.

$$\left\{ \begin{array}{c} \frac{\partial}{\partial x}\left[\frac{k_{(\alpha,b)_x}}{\mu}\frac{\partial^{1-\alpha}}{\partial t}\left(\frac{\partial p_f}{\partial x}\right)\right]+\frac{\partial}{\partial y}\left[\frac{k_{(\alpha,b)_y}}{\mu}\frac{\partial^{1-\alpha}}{\partial t}\left(\frac{\partial p_f}{\partial y}\right)\right] \\ \\ +\frac{\partial}{\partial z}\left[\frac{k_{(\alpha,b)_z}}{\mu}\frac{\partial^{1-\alpha}}{\partial t}\left(\frac{\partial p_f}{\partial z}\right)\right]- \ \hat{q}_{m-f} \end{array} \right\} = (\phi ct)_f \frac{\partial p_f}{\partial t} \tag{A.38}$$

where $\hat{q}_{m-f}$ represents the matrix-natural fracture interaction. This transfer function is assumed to occur under pseudosteady state and is given as

$$\hat{q}_{m-f} = \sigma_{SF} \ \frac{k_m}{\mu}\left(p_f - p_m\right) \tag{A.39}$$

Following the procedure described for boundary terms in hydraulic fracture domain, incorporation of the finite difference approximation of time fractional flux law into equation A.38 results in

$$\left\{ \begin{array}{c} \frac{\partial}{\partial x}\left[\frac{k_{(\alpha,b)_x}}{\mu}\sigma_\alpha \sum_{k=1}^{n+1}\omega_k^\alpha\left[\frac{\partial p(x,t_k)}{\partial x}-\frac{\partial p(x,t_{k-1})}{\partial x}\right]\right] \\ \\ +\frac{\partial}{\partial y}\left[\frac{k_{(\alpha,b)_y}}{\mu}\sigma_\alpha \sum_{k=1}^{n+1}\omega_k^\alpha\left[\frac{\partial p(y,t_k)}{\partial y}-\frac{\partial p(y,t_{k-1})}{\partial y}\right]\right] \\ \\ +\frac{\partial}{\partial z}\left[\frac{k_{(\alpha,b)_z}}{\mu}\sigma_\alpha \sum_{k=1}^{n+1}\omega_k^\alpha\left[\frac{\partial p(x,t_k)}{\partial x}-\frac{\partial p(x,t_{k-1})}{\partial x}\right]\right] \\ \\ -\ \hat{q}_{m-f} \end{array} \right\} = (\phi ct)_f \frac{\partial p_f}{\partial t} \tag{A.40}$$

Now, equation A.40 is approximated through a finite difference scheme

$$
\left\{
\begin{array}{l}
\frac{1}{\Delta x}\left\{ \frac{k_{(\alpha,b)_{i+1/2}}}{\mu}\sigma_\alpha\ \omega_{n+1}^{\alpha}\left[\frac{P_{f_{i+1}}^{n+1}-P_{f_i}^{n+1}}{\Delta x_{i+1/2}}-\frac{P_{f_{i+1}}^{n}-P_{f_i}^{n}}{\Delta x_{i+1/2}}\right]\right. \\
\quad +\frac{k_{(\alpha,b)_{i+1/2}}}{\mu}\sigma_\alpha \sum_{r=1}^{n}\omega_r^{\alpha}\left[\frac{P_{f_{i+1}}^{r}-P_{f_i}^{r}-P_{f_{i+1}}^{r-1}+P_{f_i}^{r-1}}{\Delta x_{i+1/2}}\right] \\
\quad -\frac{k_{(\alpha,b)_{i-1/2}}}{\mu}\sigma_\alpha\ \omega_{n+1}^{\alpha}\left[\frac{P_{f_i}^{n+1}-P_{f_{i-1}}^{n+1}}{\Delta x_{i-1/2}}-\frac{P_{f_i}^{n}-P_{f_{i-1}}^{n}}{\Delta x_{i-1/2}}\right] \\
\left.\quad -\frac{k_{(\alpha,b)_{i-1/2}}}{\mu}\sigma_\alpha \sum_{r=1}^{n}\omega_r^{\alpha}\left[\frac{P_{f_i}^{r}-P_{f_{i-1}}^{r}-P_{f_i}^{r-1}+P_{f_{i-1}}^{r-1}}{\Delta x_{i-1/2}}\right]\right\} \\
+\frac{1}{\Delta y}\left\{ \frac{k_{(\alpha,b)_{j+1/2}}}{\mu}\sigma_\alpha\ \omega_{n+1}^{\alpha}\left[\frac{P_{f_{j+1}}^{n+1}-P_{f_j}^{n+1}}{\Delta x_{j+1/2}}-\frac{P_{f_{j+1}}^{n}-P_{f_j}^{n}}{\Delta x_{j+1/2}}\right]\right. \\
\quad +\frac{k_{(\alpha,b)_{j+1/2}}}{\mu}\sigma_\alpha \sum_{r=1}^{n}\omega_r^{\alpha}\left[\frac{P_{f_{j+1}}^{r}-P_{f_j}^{r}-P_{f_{j+1}}^{r-1}+P_{f_j}^{r-1}}{\Delta y_{j+1/2}}\right] \\
\quad -\frac{k_{(\alpha,b)_{j-1/2}}}{\mu}\sigma_\alpha\ \omega_{n+1}^{\alpha}\left[\frac{P_{f_j}^{n+1}-P_{f_{j-1}}^{n+1}}{\Delta y_{j-1/2}}-\frac{P_{f_j}^{n}-P_{f_{j-1}}^{n}}{\Delta y_{j-1/2}}\right] \\
\left.\quad -\frac{k_{(\alpha,b)_{j-1/2}}}{\mu}\sigma_\alpha \sum_{r=1}^{n}\omega_r^{\alpha}\left[\frac{P_{f_j}^{r}-P_{f_{j-1}}^{r}-P_{f_j}^{r-1}+P_{f_{j-1}}^{r-1}}{\Delta y_{j-1/2}}\right]\right\} \\
+\frac{1}{\Delta z}\left\{ \frac{k_{(\alpha,b)_{k+1/2}}}{\mu}\sigma_\alpha\ \omega_{n+1}^{\alpha}\left[\frac{P_{f_{k+1}}^{n+1}-P_{f_k}^{n+1}}{\Delta x_{k+1/2}}-\frac{P_{f_{k+1}}^{n}-P_{f_k}^{n}}{\Delta x_{k+1/2}}\right]\right. \\
\quad +\frac{k_{(\alpha,b)_{k+1/2}}}{\mu}\sigma_\alpha \sum_{r=1}^{n}\omega_r^{\alpha}\left[\frac{P_{f_{k+1}}^{r}-P_{f_k}^{r}-P_{f_{k+1}}^{r-1}+P_{f_k}^{r-1}}{\Delta z_{k+1/2}}\right] \\
\quad -\frac{k_{(\alpha,b)_{k-1/2}}}{\mu}\sigma_\alpha\ \omega_{n+1}^{\alpha}\left[\frac{P_{f_k}^{n+1}-P_{f_{k-1}}^{n+1}}{\Delta z_{k-1/2}}-\frac{P_{f_k}^{n}-P_{f_{k-1}}^{n}}{\Delta z_{k-1/2}}\right] \\
\left.\quad -\frac{k_{(\alpha,b)_{k-1/2}}}{\mu}\sigma_\alpha \sum_{r=1}^{n}\omega_r^{\alpha}\left[\frac{P_{f_k}^{r}-P_{f_{k-1}}^{r}-P_{f_k}^{r-1}+P_{f_{k-1}}^{r-1}}{\Delta z_{k-1/2}}\right]\right\} \\
\quad -\ \hat{q}_{m-f}
\end{array}
\right\}
= \frac{(\phi ct)_{f_{i,j,k}}}{\Delta t^n}\ \left(P_{f_{i,j,k}}^{n+1}-P_{f_{i,j,k}}^{n}\right)
\tag{A.41}
$$

Multiplying equation A.41 by rock volume and defining the following transmisibility coefficients

$$E_{f_{i,j,k}} = \frac{\Delta y_j \ \Delta z_k}{\Delta x_{i+1/2}} \ \frac{k_{(\alpha,b)_{i+1/2}}}{\mu} \ \sigma_\alpha \tag{A.42}$$

$$W_{f_{i,j,k}} = \frac{\Delta y_j \ \Delta z_k}{\Delta x_{i-1/2}} \ \frac{k_{(\alpha,b)_{i-1/2}}}{\mu} \ \sigma_\alpha \tag{A.43}$$

$$F_{f_{i,j,k}} = \frac{\Delta x_i \ \Delta z_k}{\Delta y_{j+1/2}} \ \frac{k_{(\alpha,b)_{j+1/2}}}{\mu} \ \sigma_\alpha \tag{A.44}$$

$$B_{f_{i,j,k}} = \frac{\Delta x_i \ \Delta z_k}{\Delta y_{j-1/2}} \ \frac{k_{(\alpha,b)_{j-1/2}}}{\mu} \ \sigma_\alpha \tag{A.45}$$

$$N_{f_{i,j,k}} = \frac{\Delta x_i \ \Delta y_j}{\Delta z_{k+1/2}} \ \frac{k_{(\alpha,b)_{k+1/2}}}{\mu} \ \sigma_\alpha \tag{A.46}$$

$$S_{f_{i,j,k}} = \frac{\Delta x_i \ \Delta y_j}{\Delta z_{k-1/2}} \ \frac{k_{(\alpha,b)_{k-1/2}}}{\mu} \ \sigma_\alpha \tag{A.47}$$

equation A.41 can be written as

$$
\left\{
\begin{array}{c}
E_{f_{i,j,k}}\ \omega_{n+1}^{\alpha}\left[P_{f_{i+1}}^{n+1}-P_{f_i}^{n+1}-P_{f_{i+1}}^{n}+P_{f_i}^{n}\right] \\
+\ E_{f_{i,j,k}}\sum_{r=1}^{n}\omega_r^{\alpha}\left[P_{f_{i+1}}^{r}-P_{f_i}^{r}-P_{f_{i+1}}^{r-1}+P_{f_i}^{r-1}\right] \\
-\ W_{f_{i,j,k}}\ \omega_{n+1}^{\alpha}\left[P_{f_i}^{n+1}-P_{f_{i-1}}^{n+1}-P_{f_i}^{n}+P_{f_{i-1}}^{n}\right] \\
-\ W_{f_{i,j,k}}\sum_{r=1}^{n}\omega_r^{\alpha}\left[P_{f_i}^{r}-P_{f_{i-1}}^{r}-P_{f_i}^{r-1}+P_{f_{i-1}}^{r-1}\right] \\
+\ F_{f_{i,j,k}}\omega_{n+1}^{\alpha}\left[P_{f_{j+1}}^{n+1}-P_{f_j}^{n+1}-P_{f_{j+1}}^{n}+P_{f_j}^{n}\right] \\
+\ F_{f_{i,j,k}}\sum_{r=1}^{n}\omega_r^{\alpha}\left[P_{f_{j+1}}^{r}-P_{f_j}^{r}-P_{f_{j+1}}^{r-1}+P_{f_j}^{r-1}\right] \\
-\ B_{f_{i,j,k}}\ \omega_{n+1}^{\alpha}\left[P_{f_j}^{n+1}-P_{f_{j-1}}^{n+1}-P_{f_j}^{n}+P_{f_{j-1}}^{n}\right] \\
-\ B_{f_{i,j,k}}\sum_{r=1}^{n}\omega_r^{\alpha}\left[P_{f_j}^{r}-P_{f_{j-1}}^{r}-P_{f_j}^{r-1}+P_{f_{j-1}}^{r-1}\right] \\
+\ N_{f_{i,j,k}}\omega_{n+1}^{\alpha}\left[P_{f_{k+1}}^{n+1}-P_{f_k}^{n+1}-P_{f_{k+1}}^{n}+P_{f_k}^{n}\right] \\
+\ N_{f_{i,j,k}}\sum_{r=1}^{n}\omega_r^{\alpha}\left[P_{f_{k+1}}^{r}-P_{f_k}^{r}-P_{f_{k+1}}^{r-1}+P_{f_k}^{r-1}\right] \\
-\ S_{f_{i,j,k}}\ \omega_{n+1}^{\alpha}\left[P_{f_k}^{n+1}-P_{f_{k-1}}^{n+1}-P_{f_k}^{n}+P_{f_{k-1}}^{n}\right] \\
-\ S_{f_{i,j,k}}\sum_{r=1}^{n}\omega_r^{\alpha}\left[P_{f_k}^{r}-P_{f_{k-1}}^{r}-P_{f_k}^{r-1}+P_{f_{k-1}}^{r-1}\right] \\
-Vr_{i,j,k}\ \hat{q}_{m-f}
\end{array}
\right\}
=\frac{Vr_{i,j,k}(\phi ct)_{f_{i,j,k}}}{\Delta t^n}\ \left(P_{f_{i,j,k}}^{n+1}-P_{f_{i,j,k}}^{n}\right). \tag{A.48}
$$

Now equation A.48 is rearranged by separating known from unknown values

$$\left\{\begin{array}{c} E_{f_{i,j,k}}\ \omega_{n+1}^{\alpha} P_{f}{}_{i+1}^{n+1} + \ F_{f_{i,j,k}}\ \omega_{n+1}^{\alpha}\ P_{f}{}_{j+1}^{n+1} + \ N_{f_{i,j,k}}\ \omega_{n+1}^{\alpha}\ P_{f}{}_{k+1}^{n+1} \\ - \ \left(E + \ F + \ N + \ W + \ B + \ S + \ \frac{Vr\ (\phi ct)}{\Delta t^{n}\ \omega_{n+1}^{\alpha}}\right)_{f_{i,j,k}}\ \omega_{n+1}^{\alpha}\ P_{f}{}_{i,j,k}^{n+1} \\ -Vr_{i,j,k}\ \hat{q}_{m-f} + \ W_{f_{i,j,k}}\ \omega_{n+1}^{\alpha} P_{f}{}_{i-1}^{n+1} + \ B_{f_{i,j,k}}\ \omega_{n+1}^{\alpha}\ P_{f}{}_{j-1}^{n+1} + \ S_{f_{i,j,k}}\ \omega_{n+1}^{\alpha}\ P_{f}{}_{k-1}^{n+1} \\ = E_{f_{i,j,k}}\ \omega_{n+1}^{\alpha}\ \left[P_{f}{}_{i+1}^{n} - P_{f}{}_{i}^{n}\right] - E_{f_{i,j,k}} \sum_{r=1}^{n} \omega_{r}^{\alpha} \left[P_{f}{}_{i+1}^{r} - P_{f}{}_{i}^{r} - P_{f}{}_{i+1}^{r-1} + P_{f}{}_{i}^{r-1}\right] \\ +W_{f_{i,j,k}}\ \omega_{n+1}^{\alpha} \left[P_{f}{}_{i}^{n} - P_{f}{}_{i-1}^{n}\right] - W_{f_{i,j,k}} \sum_{r=1}^{n} \omega_{r}^{\alpha} \left[P_{f}{}_{i}^{r} - P_{f}{}_{i-1}^{r} - P_{f}{}_{i}^{r-1} + P_{f}{}_{i-1}^{r-1}\right] \\ +F_{f_{i,j,k}} \omega_{n+1}^{\alpha} \left[P_{f}{}_{j+1}^{n} - P_{f}{}_{j}^{n}\right] - F_{f_{i,j,k}} \sum_{r=1}^{n} \omega_{r}^{\alpha} \left[P_{f}{}_{j+1}^{r} - P_{f}{}_{j}^{r} - P_{f}{}_{j+1}^{r-1} + P_{f}{}_{j}^{r-1}\right] \\ +B_{f_{i,j,k}}\ \omega_{n+1}^{\alpha} \left[P_{f}{}_{j}^{n} - P_{f}{}_{j-1}^{n}\right] - B_{f_{i,j,k}} \sum_{r=1}^{n} \omega_{r}^{\alpha} \left[P_{f}{}_{j}^{r} - P_{f}{}_{j-1}^{r} - P_{f}{}_{j}^{r-1} + P_{f}{}_{j-1}^{r-1}\right] \\ +N_{f_{i,j,k}} \omega_{n+1}^{\alpha} \left[P_{f}{}_{k+1}^{n} - P_{f}{}_{k}^{n}\right] - N_{f_{i,j,k}} \sum_{r=1}^{n} \omega_{r}^{\alpha} \left[P_{f}{}_{k+1}^{r} - P_{f}{}_{k}^{r} - P_{f}{}_{k+1}^{r-1} + P_{f}{}_{k}^{r-1}\right] \\ +S_{f_{i,j,k}}\ \omega_{n+1}^{\alpha} \left[P_{f}{}_{k}^{n} - P_{f}{}_{k-1}^{n}\right] - S_{f_{i,j,k}} \sum_{r=1}^{n} \omega_{r}^{\alpha} \left[P_{f}{}_{k}^{r} - P_{f}{}_{k-1}^{r} - P_{f}{}_{k}^{r-1} + P_{f}{}_{k-1}^{r-1}\right] \\ -\frac{Vr_{i,j,k}\ (\phi ct)_{f_{i,j,k}}}{\Delta t^{n}}\ P_{f}{}_{i,j,k}^{n} \end{array}\right\}. \tag{A.49}$$

Now, the term $\hat{q}_{m-f}$ depends on fracture and matrix pressure, the following procedure is performed to reduce the unkowns on the system, and work only with fracture pressures. Matrix pressure will be further computed in a explicit way.

The governing equation for matrix blocks is given by

$$\hat{q}_{m-f} = (\phi ct)_{m} \frac{\partial p_{m}}{\partial t}. \tag{A.50}$$

Combining the discrete form of equation A.39 and equation A.50 results in

$$\sigma_{SF}\ \frac{k_{mi,j,k}}{\mu} \left(P_{f}{}_{i,j,k}^{n+1} - P_{m}{}_{i,j,k}^{n+1}\right) = \frac{(\phi ct)_{f_{i,j,k}}}{\Delta t^{n}} \left(P_{m}{}_{i,j,k}^{n+1} - P_{m}{}_{i,j,k}^{n}\right), \tag{A.51}$$

rearranging the previous equation

$$\left[\frac{k_{mi,j,k}}{\mu}+\frac{(\phi ct)_{f_{i,j,k}}}{\Delta t^n}\right]P_{m}{}_{i,j,k}^{n+1}=\frac{k_{mi,j,k}}{\mu}P_{f}{}_{i,j,k}^{n+1}+\frac{(\phi ct)_{f_{i,j,k}}}{\Delta t^n}P_{m}{}_{i,j,k}^{n}, \tag{A.52}$$

solving the equation for $P_{m}{}_{i,j,k}^{n+1}$

$$P_{m}{}_{i,j,k}^{n+1}=\frac{k_{mi,j,k}\ \sigma_{SF}\ \Delta t^n P_{f}{}_{i,j,k}^{n+1}\ +\ (\phi ct)_{mi,j,k}\ \mu\ P_{m}{}_{i,j,k}^{n}}{k_{mi,j,k}\ \sigma_{SF}\ \Delta t^n\ +(\phi ct)_{mi,j,k}\ \mu}. \tag{A.53}$$

Substitution of A.53 into the discrete form of equation A.39 results in

$$\hat{q}_{m-f_{i,j,k}}^{n+1}=\sigma_{SF}\ \frac{k_{mi,j,k}}{\mu}\left[P_{f}{}_{i,j,k}^{n+1}-\frac{k_{mi,j,k}\ \sigma_{SF}\ \Delta t^n P_{f}{}_{i,j,k}^{n+1}\ +\ (\phi ct)_{mi,j,k}\ \mu\ P_{m}{}_{i,j,k}^{n}}{k_{mi,j,k}\ \sigma_{SF}\ \Delta t^n\ +(\phi ct)_{mi,j,k}\ \mu}\right], \tag{A.54}$$

grouping similar terms some members are canceled

$$\hat{q}_{m-f_{i,j,k}}^{n+1}=\sigma_{SF}\ \frac{k_{mi,j,k}}{\mu}\left[\frac{(\phi ct)_{mi,j,k}\ \mu\ P_{f}{}_{i,j,k}^{n+1}-\ (\phi ct)_{mi,j,k}\ \mu\ P_{m}{}_{i,j,k}^{n}}{k_{mi,j,k}\ \sigma_{SF}\ \Delta t^n\ +(\phi ct)_{mi,j,k}\ \mu}\right], \tag{A.55}$$

finally, the discrete form of the transfer function ($\hat{q}_{m-f}$) can be written as

$$\hat{q}_{m-f_{i,j,k}}^{n+1}=\left[\frac{k_{mi,j,k}\ \sigma_{SF}\ \ (\phi ct)_{mi,j,k}\ P_{f}{}_{i,j,k}^{n+1}-\ k_{mi,j,k}\ \sigma_{SF}\ \ (\phi ct)_{mi,j,k}\ P_{m}{}_{i,j,k}^{n}}{k_{mi,j,k}\ \sigma_{SF}\ \Delta t^n\ +(\phi ct)_{mi,j,k}\ \mu}\right]. \tag{A.56}$$

Now, the previous equation is substituted into equation A.49. By grouping similar terms, one more coefficient (C) and the known values vector (R) can be defined. The equation A.49 can be written in the following compact form

$$\left\{\begin{array}{c} E_{f_{i,j,k}}\ \omega_{n+1}^{\alpha}P_{f}{}_{i+1}^{n+1}+\ F_{f_{i,j,k}}\ \omega_{n+1}^{\alpha}\ P_{f}{}_{j+1}^{n+1}+\ N_{f_{i,j,k}}\ \omega_{n+1}^{\alpha}\ P_{f}{}_{k+1}^{n+1} \\ \\ +\ C_{f_{i,j,k}}\ \omega_{n+1}^{\alpha}\ P_{f}{}_{i,j,k}^{n+1} \\ \\ +\ W_{f_{i,j,k}}\ \omega_{n+1}^{\alpha}P_{f}{}_{i-1}^{n+1}+\ B_{f_{i,j,k}}\ \omega_{n+1}^{\alpha}\ P_{f}{}_{j-1}^{n+1}+\ S_{f_{i,j,k}}\ \omega_{n+1}^{\alpha}\ P_{f}{}_{k-1}^{n+1} \end{array}\right\}=R_{f_{i,j,k}} \tag{A.57}$$

where

$$C_{f_{i,j,k}} = -\left[E + F + N + W + B + S\right]_{i,j,k} - \frac{1}{\omega_r^\alpha}\frac{Vr\,(\phi ct)}{\Delta t^n \omega_{n+1}^\alpha} + \frac{Vr\ k_m\sigma_{SF}\ (\phi ct)_m}{k_m\sigma_{SF}\Delta t^n + \mu\,(\phi ct)_m} \quad \text{(A.58)}$$

and

$$R_{f_{i,j,k}} = \left\{ \begin{array}{c} E_{f_{i,j,k}}\ \omega_{n+1}^\alpha\ \left[P_{f_{i+1}}^n - P_{f_i}^n\right] - E_{f_{i,j,k}} \sum_{r=1}^n \omega_r^\alpha \left[P_{f_{i+1}}^r - P_{f_i}^r - P_{f_{i+1}}^{r-1} + P_{f_i}^{r-1}\right] \\ +W_{f_{i,j,k}}\ \omega_{n+1}^\alpha \left[P_{f_i}^n - P_{f_{i-1}}^n\right] - W_{f_{i,j,k}} \sum_{r=1}^n \omega_r^\alpha \left[P_{f_i}^r - P_{f_{i-1}}^r - P_{f_i}^{r-1} + P_{f_{i-1}}^{r-1}\right] \\ +F_{f_{i,j,k}}\omega_{n+1}^\alpha \left[P_{f_{j+1}}^n - P_{f_j}^n\right] - F_{f_{i,j,k}} \sum_{r=1}^n \omega_r^\alpha \left[P_{f_{j+1}}^r - P_{f_j}^r - P_{f_{j+1}}^{r-1} + P_{f_j}^{r-1}\right] \\ +B_{f_{i,j,k}}\ \omega_{n+1}^\alpha \left[P_{f_j}^n - P_{f_{j-1}}^n\right] - B_{f_{i,j,k}} \sum_{r=1}^n \omega_r^\alpha \left[P_{f_j}^r - P_{f_{j-1}}^r - P_{f_j}^{r-1} + P_{f_{j-1}}^{r-1}\right] \\ +N_{f_{i,j,k}}\omega_{n+1}^\alpha \left[P_{f_{k+1}}^n - P_{f_k}^n\right] - N_{f_{i,j,k}} \sum_{r=1}^n \omega_r^\alpha \left[P_{f_{k+1}}^r - P_{f_k}^r - P_{f_{k+1}}^{r-1} + P_{f_k}^{r-1}\right] \\ +S_{f_{i,j,k}}\ \omega_{n+1}^\alpha \left[P_{f_k}^n - P_{f_{k-1}}^n\right] - S_{f_{i,j,k}} \sum_{r=1}^n \omega_r^\alpha \left[P_{f_k}^r - P_{f_{k-1}}^r - P_{f_k}^{r-1} + P_{f_{k-1}}^{r-1}\right] \\ -\frac{Vr_{i,j,k}\ (\phi ct)_{f_{i,j,k}}}{\Delta t^n}\ P_{f_{i,j,k}}^n - \left(\frac{Vr\ k_m\sigma_{SF}\ (\phi ct)_m}{k_m\sigma_{SF}\Delta t^n + \mu(\phi ct)_m}\right)_{i,j,k} P_{m_{i,j,k}}^n \end{array} \right\} \quad \text{(A.59)}$$

Finally, equation A.57 represents the governing equation describing flow through the region outside the hydraulic fracture.

Appendix B

Finite-Difference Approximation of Flux Equation

The following derivation is based on the methodology presented by Murio (2008), Holy (2016) and Holy and Ozkan (2017).
Lets consider the time-fractional flux equation in x direction

$$\hat{q}_{F-SRV_x}\Big|_{L_{Fx}} = -\frac{k_{(\alpha,b)_x}}{\mu}\frac{\partial^{1-\alpha}}{\partial t}\left(\frac{\partial p}{\partial x}\right)\Big|_{L_{Fx}}. \tag{B.1}$$

Time fractional derivative is defined according to Caputo (1967), thus

$$\left[\frac{\partial^{1-\alpha}}{\partial t^{1-\alpha}}\left(\frac{\partial p}{\partial x}\right)\right] = \frac{1}{\Gamma(\alpha)}\int_0^{t_{n+1}}\frac{\partial}{\partial \tau}\left(\frac{\partial p}{\partial x}\right)(t_{n+1}-\tau)^{-(1-\alpha)}\ d\tau. \tag{B.2}$$

The integral in equation B.2 is approximated by integrating smaller intervals which are later summed together. Each one of these new integrals encompasses a time lapse $\Delta t_r = t_{r-1} - t_r$

$$\left[\frac{\partial^{1-\alpha}}{\partial t^{1-\alpha}}\left(\frac{\partial p}{\partial x}\right)\right] = \frac{1}{\Gamma(\alpha)}\sum_{r=1}^{n+1}\int_{t_{r-1}}^{t_r}\frac{\partial}{\partial \tau}\left(\frac{\partial p}{\partial x}\right)(t_{n+1}-\tau)^{-(1-\alpha)}\ d\tau. \tag{B.3}$$

Now, a backward difference is used to approximate the derivative inside each integral

$$\left[\frac{\partial^{1-\alpha}}{\partial t^{1-\alpha}}\left(\frac{\partial p}{\partial x}\right)\right] = \frac{1}{\Gamma(\alpha)}\sum_{r=1}^{n+1}\int_{t_{r-1}}^{t_r}\frac{\frac{\partial p(x,t_r)}{\partial x} - \frac{\partial p(x,t_{r-1})}{\partial x}}{\Delta t_r}\left(t_{n+1}-\tau\right)^{-(1-\alpha)}\ d\tau, \tag{B.4}$$

note that the integration variable is τ, thus some terms can be extracted from integral

$$\left[\frac{\partial^{1-\alpha}}{\partial t^{1-\alpha}}\left(\frac{\partial p}{\partial x}\right)\right] = \frac{1}{\Gamma(\alpha)}\sum_{r=1}^{n+1}\left[\frac{\frac{\partial p(x,t_r)}{\partial x} - \frac{\partial p(x,t_{r-1})}{\partial x}}{\Delta t_r}\right]\int_{t_{r-1}}^{t_r}\left(t_{n+1}-\tau\right)^{-(1-\alpha)}\ d\tau, \tag{B.5}$$

the remaining terms are integrated next

$$\begin{aligned}\int_{t_{r-1}}^{t_r}\left(t_{n+1}-\tau\right)^{(-1+\alpha)}\ d\tau &= -\frac{\left[t_{n+1}-\tau\right]^{\alpha}}{\alpha}\Bigg|_{t_{r-1}}^{t_r}\\ &= -\frac{\left[t_{n+1}-t_r\right]^{\alpha}+\left[t_{n+1}-t_{r-1}\right]^{\alpha}}{\alpha}\\ &= \frac{1}{\alpha}\Big[\left[t_{n+1}-t_{r-1}\right]^{\alpha}-\left[t_{n+1}-t_r\right]^{\alpha}\Big].\end{aligned} \tag{B.6}$$

Substitution of equation B.6 into equation B.5 results in

$$\left[\frac{\partial^{1-\alpha}}{\partial t^{1-\alpha}}\left(\frac{\partial p}{\partial x}\right)\right] = \frac{1}{\Gamma(\alpha)}\sum_{r=1}^{n+1}\left[\frac{\frac{\partial p(x,t_r)}{\partial x} - \frac{\partial p(x,t_{r-1})}{\partial x}}{\Delta t_r}\right]\frac{1}{\alpha}\Big[\left[t_{n+1}-t_{r-1}\right]^{\alpha}-\left[t_{n+1}-t_r\right]^{\alpha}\Big] \tag{B.7}$$

recalling gamma function properties,

$$\left[\frac{\partial^{1-\alpha}}{\partial t^{1-\alpha}}\left(\frac{\partial p}{\partial x}\right)\right] = \frac{1}{\Gamma(\alpha+1)}\sum_{r=1}^{n+1}\left[\frac{\frac{\partial p(x,t_r)}{\partial x} - \frac{\partial p(x,t_{r-1})}{\partial x}}{\Delta t_r}\right]\Big[\left[t_{n+1}-t_{r-1}\right]^{\alpha}-\left[t_{n+1}-t_r\right]^{\alpha}\Big]. \tag{B.8}$$

Finally, the compact form of the finite-difference approximation to time-fractional derivative is given by

$$\left[\frac{\partial^{1-\alpha}}{\partial t^{1-\alpha}}\left(\frac{\partial p}{\partial x}\right)\right] = \sigma_\alpha \sum_{r=1}^{n+1} \omega_k^\alpha \left[\frac{\partial p\left(x,t_r\right)}{\partial x} - \frac{\partial p\left(x,t_{r-1}\right)}{\partial x}\right], \tag{B.9}$$

where

$$\sigma_\alpha = \frac{1}{\Gamma\left(\alpha+1\right)}, \tag{B.10}$$

and

$$\omega_k^\alpha = \frac{\left[t_{n+1}-t_{r-1}\right]^\alpha - \left[t_{n+1}-t_r\right]^\alpha}{\Delta t_r}. \tag{B.11}$$

This approximation to time-fractional derivative is introduced into the flux equation

$$\hat{q}_{F-SRV_x} = -\frac{k_{\alpha,b_x}}{\mu}\ \sigma_\alpha \sum_{r=1}^{n+1} \omega_k^\alpha \left[\frac{\partial p\left(x,t_r\right)}{\partial x} - \frac{\partial p\left(x,t_{r-1}\right)}{\partial x}\right]. \tag{B.12}$$